

University of New Mexico

UNM Digital Repository

Biomedical Engineering ETDs

Engineering ETDs

Summer 7-12-2021

Correlating Diffusional Dynamics and Receptor Tyrosine Kinase Function Using Single Quantum Dot Tracking

Irais Ortiz Caraveo
University of New Mexico

Follow this and additional works at: https://digitalrepository.unm.edu/bme_etds



Part of the [Molecular, Cellular, and Tissue Engineering Commons](#)

Recommended Citation

Ortiz Caraveo, Irais. "Correlating Diffusional Dynamics and Receptor Tyrosine Kinase Function Using Single Quantum Dot Tracking." (2021). https://digitalrepository.unm.edu/bme_etds/39

This Thesis is brought to you for free and open access by the Engineering ETDs at UNM Digital Repository. It has been accepted for inclusion in Biomedical Engineering ETDs by an authorized administrator of UNM Digital Repository. For more information, please contact disc@unm.edu.

Irais Ortiz Caraveo

Candidate

Biomedical Engineering Program, School of Engineering

Department

This thesis is approved, and it is acceptable in quality and form for publication:

Approved by the Thesis Committee:

Diane Lidke, Chairperson

Heather Canavan

Linnea Ista

**Correlating Diffusional Dynamics and Receptor Tyrosine Kinase Function Using Single
Quantum Dot Tracking**

BY

IRAIS ORTIZ CARAVEO

**BACHELOR OF ARTS
SPANISH**

**BACHELOR OF SCIENCE
CHEMICAL AND BIOLOGICAL ENGINEERING**

THESIS

Submitted in Partial Fulfillment of the
Requirements for the Degree of

Master of Science

Biomedical Engineering

The University of New Mexico
Albuquerque, New Mexico

July, 2021

DEDICATION

En memoria de Ever Ivan Manjarrez Caraveo, la inspiración de mi corazón.

ACKNOWLEDGEMENTS

I heartily acknowledge Diane Lidke, my advisor and chairperson for being a constant source of inspiration and for her continuous and unconditional support through the years. Her compassion, guidance and leadership skills will remain with me as I continue my career.

I also want to thank my committee members, Dr. Ista and Dr. Canavan for their valuable advice pertaining to my academic and professional career. Their encouragement, bravery, and ability to lead by example inspired and encouraged me to continue my education.

My gratitude is extended to Elon Jahmba and Carolina Franco Nitta, two mentors, and now friends, who invested great portions of their time training and mentoring me, thank you for your patience and kindness. Also, thank you to Shayna Lucero, Will Kanagy, Derek Rinaldi, Mara Steinkamp, Danielle Burke and Rachel Grattan for their willingness to help in any way they could.

To Keith Lidke's lab, thank you for collaborating with me on the analysis portion of this study and for sharing your valuable knowledge and tools.

A huge thank you to my life mentor, Stanley Lewis whose multifaceted and unwavering support facilitated my studies in a multitude of ways.

A mi madre y a mi padre, gracias por su valentia al abandonar sus vidas para darme la oportunidad de presegir mis sueños. E aqui la culminación de uno de ellos. To my brother, thank you for sparking my curiosity with your marvelous questions.

And finally, but most importantly, thank you to my husband, your love and unconditional support is the greatest gift of all. Thank you for making this possible.

Correlating Diffusional Dynamics and Receptor Tyrosine Kinase Function Using Single Quantum Dot Tracking

by

IRAIS ORTIZ CARAVEO

B.A., Spanish, University of New Mexico, 2020

B.Sc., Chemical & Biological Engineering, University of New Mexico, 2020

M.Sc., Biomedical Engineering, University of New Mexico 2021

ABSTRACT

Epidermal growth factor receptor (EGFR) signal transduction is initiated via ligand (EGF) binding, followed by dimerization, autophosphorylation of the C-terminal tails, and recruitment of proteins that form a larger signaling complex to propagate the signal. We explored the relationship between receptor mobility and signaling using single-particle tracking (SPT) by examining the diffusional dynamics of EGFR and two truncation mutants to understand whether mobility changes are correlated with signaling. Results revealed that phosphorylation of the C-terminal tail of EGFR is required for maximal reduction in mobility that occurs with EGF stimulation, indicating that receptor mobility is a read-out for receptor signaling. Additionally, this study looks at the relationship between EGFR and another membrane receptor, Recepteur d'Origine Nantis (RON), using the same approach. By tracking the diffusional dynamics of RON, we found that RON's kinase domain is not required for EGF-dependent slowdown and that EGFR phosphorylates RON to propagate crosstalk.

TABLE OF CONTENTS

LIST OF FIGURES	viii
LIST OF TABLES	x
CHAPTER 1	1
INTRODUCTION	1
Receptor Tyrosine Kinases (RTKs).....	1
Epidermal Growth Factor Receptor (EGFR)	3
Récepteur d'Origine Nantais (RON).....	10
Fluorescence microscopy & Single Particle Tracking (SPT)	12
Mean Square Displacement (MSD) and Diffusion.....	16
HMM two color imaging analysis (dimerization measurement)	17
Thesis scope and aims.....	17
CHAPTER 2	20
METHODS	20
Biochemical Methods.....	20
2.1.1 <i>Cell lines and Reagents.....</i>	<i>20</i>
2.1.2 <i>HeLa CCL2 Shc1/Grb2 KO</i>	<i>21</i>
2.1.3 <i>Plasmid cloning, cell transfections</i>	<i>21</i>
2.1.4 <i>Immunofluorescence staining</i>	<i>21</i>
2.1.5 <i>Cell Sorting</i>	<i>22</i>
2.1.6 <i>Multiplex Immunoblotting.....</i>	<i>22</i>
Microscopy and mathematical methods	23
2.1.7 <i>Microscope & camera set-up.....</i>	<i>23</i>
2.1.8 <i>Live cell imaging.....</i>	<i>24</i>
2.1.9 <i>Single Particle Tracking (SPT).....</i>	<i>25</i>

2.1.10	<i>Mean Square Displacement (MSD)</i>	26
2.1.11	<i>Hidden Markov Model (HMM)</i>	26
2.1.12	<i>Rate parameter estimation</i>	28
2.1.13	<i>Statistical analysis</i>	29
CHAPTER 3	30
RESULTS AND DISCUSSION	30
Cell line generation & characterization	30
Overview of SPT data presentation		36
Role of adaptor proteins in EGFR's mobility: Grb2 & Shc1		36
EGFR truncation mutants' contribution to EGFR mobility		42
EGFR HMM Preliminary Results		51
EGFR-RON crosstalk		54
CHAPTER 4	66
SUMMARY	66
CHAPTER 5	69
FUTURE DIRECTIONS	69
REFERENCES		70

LIST OF FIGURES

Figure 1. RTK signaling overview.	3
Figure 2. EGFR dimerization.	5
Figure 3. EGFR mediated RAS activation.	7
Figure 4. EGFR KO and Truncation Mutants.	9
Figure 5. RON signaling overview.	10
Figure 6. EGFR-RON Crosstalk.	12
Figure 7. Schematic representation of the optical set up for SPT.	13
Figure 8. HA-EGFR QD labeling.	15
Figure 9. Schematic representation of trajectory formation.	16
Figure 10. EGFR & EGFR mutant cartoon.	30
Figure 11. Cell line sorting and immunofluorescence results for expression verification.	34
Figure 12. EGFR-WT, EGFR-Δ998 and EGFR-ECDTM immunoblots.	35
Figure 13. Overview of Shc1 & Grb2 protein recruitment post-dimerization.	37
Figure 14. Direct QD binding of EGFR & EGFR's kinase domain inhibition.	38
Figure 15. Plots comparing HeLa EGFR WT & Shc1/Grb2 KO \pm 10 μm Afatinib.	40

Figure 16. Diffusion coefficients for SPT of HeLa WT & Grb2/Shc1 KO QD655-EGF \pm 10 μm Afatinib.....	41
Figure 17. Plots comparing QD655- α-HA: HA-EGFR-WT, HA-EGFR-Δ998 & HA-EGFR-ECDTM \pm Dark EGF or QD655-EGF.....	46
Figure 18. Diffusion coefficients for SPT of QD655-α-HA: HA-EGFR-WT, HA-EGFR-Δ998 & HA-EGFR-ECDTM \pm Dark EGF or QD655-EGF.	48
Figure 19. Diffusion coefficients QD655-α -HA: HA-EGFR-WT, HA-EGFR-Δ998 & HA-EGFR-ECDTM \pm Dark EGF or QD655-EGF..	50
Figure 20. Depiction of HMM model states 1 and 2.	52
Figure 21. k_{off} rates of EGFR-WT, EGFRΔ998, EGFR-ECDTM \pm 400 pM QD655-EGF & QD605-EGF preliminary estimates.	53
Figure 22. Immunoblot of A431 HA RON cells were treated with 5 nM MSP, 50 nM EGF or left untreated..	56
Figure 23. HA-RON & HA- RON K1114M QD labeling.....	57
Figure 24. Plots comparing RON mobility without treatment, + 5 nM MSP, + 20 nM MSP, + 5 nM EGF, + 50 nM EGF, + 10 μm Afatinib and + 10 μm Afatinib and 5 nM EGF..	59
Figure 25. Diffusion coefficients for SPT of QD655-HA-RON in A431 HA-RON.....	60
Figure 26. Diffusion coefficients for SPT of HA-RON \pm 5 nM MSP, \pm 10 μm Afatinib, \pm 10 μm Afatinib and 5 nM MSP.....	62
Figure 27. EGFR stimulation results in RON Phosphorylation and does not require RON's kinase activity.	64
Figure 28. Diffusion coefficients for SPT of A431 HA-RON and A431 HA RON K1114 α -HA-QD655 \pm 50 nM EGF.....	65

LIST OF TABLES

Table 1. Results summary for HeLa WT and Shc1/Grb2 KO QD655-EGF ± Afatinib..42

Table 2. Results summary for QD655- α -HA: HA-EGFR-WT, HA-EGFR- Δ 998 & HA-EGFR-ECDTM ± Dark EGF or QD655-EGF or 400 pM QD655-EGF including errors and statistical analysis.. 47

Table 3. Results summary for A431 HA RON, ± 10 μ m Afatinib, ± 5 or 20 nM MSP, or ± 5 or 50 nM EGF including errors and statistical analysis.. 63

CHAPTER 1

INTRODUCTION

Centuries of studies agree that communication and cooperation are essential for human life.¹ Not surprisingly, these characteristics are equally important at the molecular level considering that humans rely heavily on molecular signaling mechanisms to facilitate life as we know it. Meticulously coordinated signaling pathways are at the center of every cellular event and involve numerous moving parts to execute the simplest of tasks. As with everything in life, imperfections arise as a result of the complexity behind mechanisms. In the context of signaling pathways, those imperfections can lead to dire outcomes such as cancer, which arises from uncontrolled cellular growth due to failures in cell regulation. Current studies aim to elucidate signaling pathways and potential sources of failures within them in hopes of revealing potential therapeutic targets to counteract those failures. This study focuses on two cell surface receptors whose signaling mechanisms are well documented in cancer studies. The aim is to better understand the mechanisms that facilitate receptor interactions to drive signaling by looking at them through a biophysical lens.

Receptor Tyrosine Kinases (RTKs)

A family of cell surface receptors known as the Receptor Tyrosine Kinase (RTK) family is comprised of growth factor transmembrane receptors with ligand-controlled tyrosine kinase activity.² RTKs are found embedded in a cell's plasma membrane and play an imperative role in signaling mechanisms. RTKs have a conserved structure consisting of an extracellular (EC) domain that binds ligands, a single-pass transmembrane (TM) domain, and a cytoplasmic kinase domain (KD). Upon ligand binding, RTKs undergo conformational

changes to initiate downstream signaling. Those structural rearrangements are often referred to as the structure-function relationship for RTK activity. **Figure 1** shows how the conformational changes that RTKs undergo ultimately elicit cellular responses. RTK responses are mainly involved in basic, but important cellular processes that are significant in development. These include cell proliferation, migration, metabolism, and differentiation, to name a few. Note that the mentioned processes are also commonly involved in uncontrolled cellular growth, making members of the RTK family, whether overexpressed or mutated, key players in the uncontrolled cellular proliferation that often leads to cancer. Further evidence of this observation lies in a study that revealed cancer patients who had an overexpression of RTKs commonly had poorer outcomes when compared to patients who did not.³ As a result of the obvious involvement that RTKs have in a variety of cancers, there has been an increased focus on RTKs as therapeutic targets.

The study of specific receptors and the roles they play in eliciting cellular responses has been an ongoing focus of the scientific community for decades. The complexity surrounding specific transmembrane proteins requires extensive research as these proteins usually serve more than one function through a variety of signaling pathways. While many mechanisms have yet to be discovered, some well-established ones still require attention due to mechanistic failures within them. The mechanistic malfunctions of independent and/or collaborating RTKs specifically, could help elucidate how they lead to diseases and reveal potential therapeutic targets. It has become increasingly difficult to isolate specific receptors as the sole cause of dire outcomes. Often, RTKs collaborate and develop therapeutic resistance, requiring multi-target therapies. Therefore, studying RTKs in combination has become just as important as studying them independently. Biochemical approaches have revealed important

details that allow us to appreciate the basic operating forms of the receptors but, those approaches are limited. They lack insight into the dynamics of RTK signaling in a cellular environment. As a result, we are left with a knowledge gap surrounding the signaling dynamics of the receptors in live cells. This study aims to narrow that knowledge gap by focusing on the diffusional dynamics of two members of the RTK family, the epidermal growth factor receptor (EGFR) and the Recepteur d'Origine Nantis (RON).

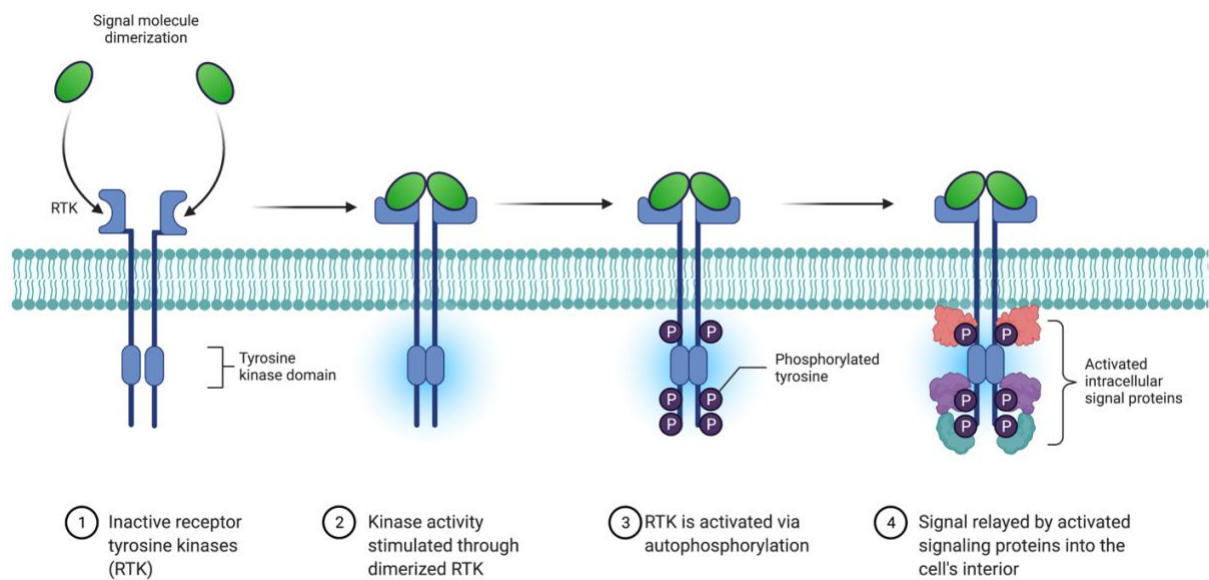


Figure 1. RTK signaling overview. Two inactive receptors, or monomers, found in the cell membrane are bound by their respective ligand. As a result, the two receptors unite (dimerize) and activate kinase activity. This results in phosphorylation of the tyrosine kinase domain leading to the signaling cascades that provoke cellular responses. (Created with BioRender.com)

Epidermal Growth Factor Receptor (EGFR)

On their search for agents involved in differentiation and growth within the embryonic nervous system, Rita Levi-Montalcini and Stanley Cohen made a peculiar observation that

would ripple through decades of research. Precocious eyelid opening in mice led to the discovery of the epidermal growth factor (EGF).⁴ It was a finding that granted them the Nobel Prize in Physiology or Medicine and led to the unveiling of the RTK family. Years of proceeding research by Cohen and others revealed that EGFR is a 170-kD, 1,186-amino-acid glycoprotein.⁵ The protein's structure was also broken up into subsections that expand the extracellular, transmembrane, and kinase domains. The collective extracellular domain, also known as the ectodomain, is composed of four parts: subdomains I, II, III, and IV. Subdomains I and III undergo structural rearrangement to create a pocket for EGF (EGFR's ligand) binding. Subsequently, a loop, (or dimerization arm) is then exposed to allow homodimerization in subdomain II.⁶ The transmembrane (TMD) and juxtamembrane domains (JMD) interact with the lipid bilayer and reinforce EGFR's structure.⁷ The tyrosine kinase domain (TKD) and C-terminal tail serve as phosphorylation and protein recruitment sites. Previous studies have found that mutations in EGFR's domains are related to specific cancer types. For example, mutations in domains I and IV are commonly found in glioblastoma, mutations in domain III with colorectal cancer, and mutations in the kinase domain with non-small cell lung cancer (NSCLC).⁸ Mutations found within the TM-JM do not seem to affect the structure but have proved to be problematic because they aid cellular proliferation in cancer; impacting the receptor's function.⁹

The classical model for EGFR activation is that upon EGF binding, also referred to as stimulation, two individual EGF molecules bind to two distinct EGFR proteins also known as monomers. Once bound, EGFR undergoes structural rearrangement, by exposing its dimerization arm to form a 1:1 EGF:EGFR stable complex before coming together to form a 2:2 EGF:EGFR dimer complex¹⁰ as shown in **Figure 2**. Various studies have shown that EGF

is not the only ligand that can activate the EGFR. Different EGFR ligands have been found to elicit different responses depending on their affinity. Low-affinity ligands such as epiregulin (EPR) and epigen (EGN) act as partial agonists and elicit a less-stable dimerization response when compared to high-affinity ligands such as EGF and transforming growth factor- α (TGF α).¹¹ Other studies have shown that dimers can form in a 1:2 EGF:EGFR complex, but those dimers are short-lived (less stable) and do not elicit the same responses as the 2:2 complexes.¹² There is also evidence that EGFR can form heterodimers with other members of the RTK family such as ErbB2, ErbB3, and ErbB4.¹³ These collaborations can hint at potential sources of therapeutic resistance. In this study, we only focus on EGF and 2:2 complexes.

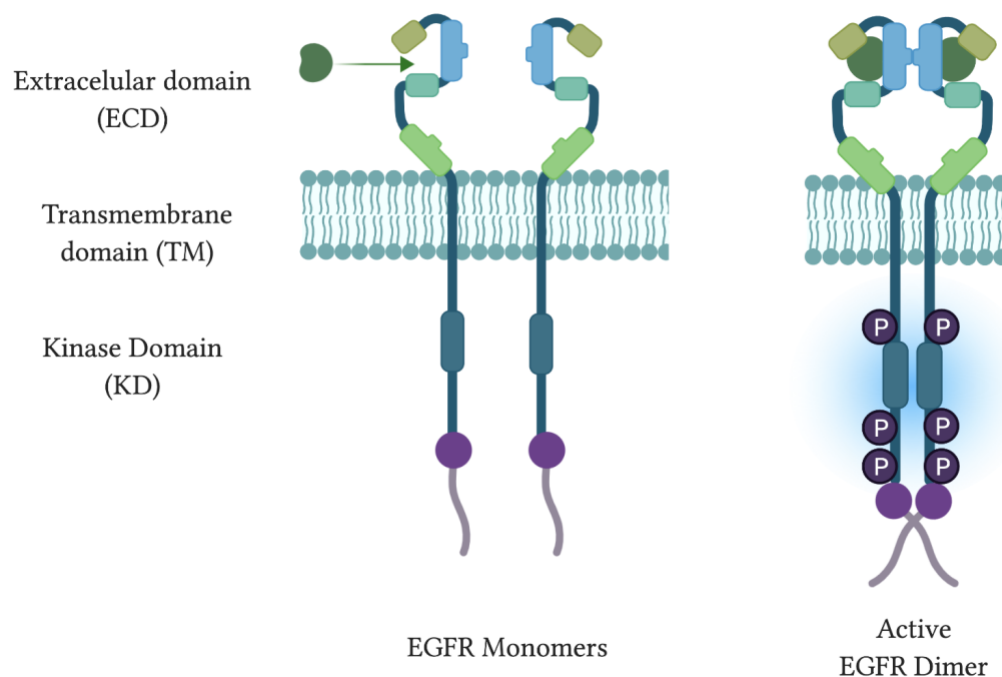


Figure 2. EGFR dimerization. EGFR dimerization is induced by EGF ligand binding EGFR to form a 1:1 EGF:EGFR complex intermediate. The intermediate then forms a 2:2 EGF:EGFR dimer, phosphorylation occurs and results in downstream signaling cascade. (Created with BioRender.com)

As previously described in section 1.2, the downstream signaling that follows dimerization can result in a cellular response that involves cell adhesion, migration, motility, survival, tumor invasion, cell cycle progression, and others.^{14,15} One well-known example of signaling mechanisms is EGFR mediated RAS activation.^{16,17} So far, biochemical approaches have determined that post-dimerization and kinase auto-phosphorylation of EGFR, binding sites for adaptor proteins Shc1 and Grb2, become available to initiate a signaling cascade.^{18,19,20,21} Subsequently, SOS is recruited, in turn, SOS binds inactive RAS, allowing it to exchange GDP for GTP.^{22,23} This exchange activates RAS kinase activity and as a result, RAS activates Raf.^{24,25} Raf then activates MEK leading to ERK activation via phosphorylation.²⁶ In combination, this series of events lead to the stimulation of transcription factors that result in gene expression²⁷ that then result in cell proliferation or even cell survival as shown in **Figure 3**. It is critical to mention that Shc1 and Grb2 participate in other signaling mechanisms that involve other proteins. Although Shc1 and Grb2 are not exclusive to the signaling mechanism described above, they were looked further into as part of this study in the context of EGFR signaling exclusively.

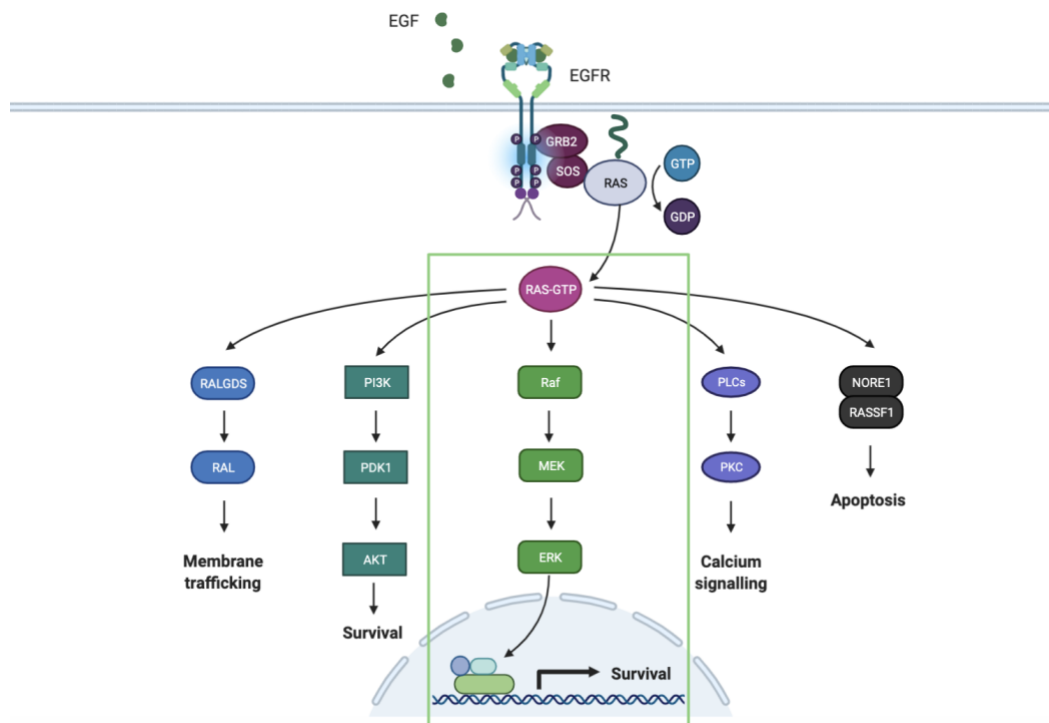


Figure 3. EGFR mediated RAS activation. One of EGFR’s signaling mechanisms involving the recruitment of Shc1 & Grb2 followed by SOS-RAS binding that allows for GDP & GTP exchange that in turn, initiates RAS activity followed by Raf & MEK activation leading to gene expression and cell survival. (Created with BioRender.com)

Although biochemical and crystallographic studies provide insight into the structure-function relationship of EGFR,^{28,29,30} they are incapable of producing any dynamic information. Most of what we know about EGFR was discovered through studies performed outside of the cell using techniques that fail to capture the EGFR’s behavior. The limitation partly arises from differences in dimensions and degrees of rotational freedom between experiments in solution versus cellular environments. This study follows the lead of more recent dynamics-focused studies^{12,31,32,33} that use sophisticated techniques such as single-particle tracking (SPT) to quantify protein mobility in live cells.

Mobility measurements, such as diffusion, have enabled further characterization of protein dynamics. When studying the dynamics of specific proteins, the interpretation of

dynamic values is still a work in progress. Two independent studies on EGFR's diffusion and dimerization predicted that a two-fold slowdown in EGFR mobility upon stimulation was indicative of dimer formation.^{31,34} Later, using 2-color single-molecule imaging techniques, Shalini *et. al* determined that it was a 6-fold decrease in EGFR mobility that characterized the formation of signaling competent dimers.³³ These three studies correlate protein mobility measurements to dimerization state. More specifically, a decreased diffusion, or slowdown in mobility, is indicative of dimerization. The discrepancy between a 2-fold and a 6-fold slowdown for dimer characterization may be due to different interpretations of the observed slowdown. Attributing a portion of the protein's slowdown to dimerization is logical but, dimerization may not be the sole cause of the diffusional slowdown that is observed. Another contributor to the observed slowdown could be protein recruitment. Thanks to extensive biochemical data, it is known that protein recruitment occurs in various EGFR signaling mechanisms.^{20,35,36,37} Protein recruitment immediately follows receptor phosphorylation and usually involves multiple proteins attaching to an EGFR dimer to form a larger and heavier complex. Classical approaches such as Newton's law of motion³⁸ and the Stokes-Einstein Equation³⁹, imply that heavier objects move more slowly. Therefore, we hypothesized that dimerization is only responsible for a portion of the slowdown but, not its entirety.

This study aims to highlight the contribution of adaptor proteins by first examining EGFR mobility in cells lacking Shc1 and Grb2 and by analysis of EGFR mutants that are incapable of cytosolic protein recruitment (shown in **Figure 4**). We recognize that Shc1 and Grb2 are not the only proteins involved in EGFR signaling mechanisms. Therefore, we took a different approach that involved comparing the mobility of EGFR and two distinct EGFR truncation mutants. One of the mutants, EGFR- Δ 998, is a form of EGFR whose C-terminal tail

was truncated. The truncation of the C-terminal removes all but one tyrosine binding site, dramatically reducing protein recruitment capabilities. The other EGFR mutant is composed of the extracellular and transmembrane domain only (ECDTM). The kinase domain and entire intracellular region of the protein were completely truncated but, the protein's ligand-binding site was left intact. We wanted to know if limiting EGFR's signaling ability would affect the slowdown in mobility upon stimulation. By doing so, not only would we be able to determine whether the diffusion output was a readout for signaling, but we would also add to our understanding of the structure-function relationship of the receptor.

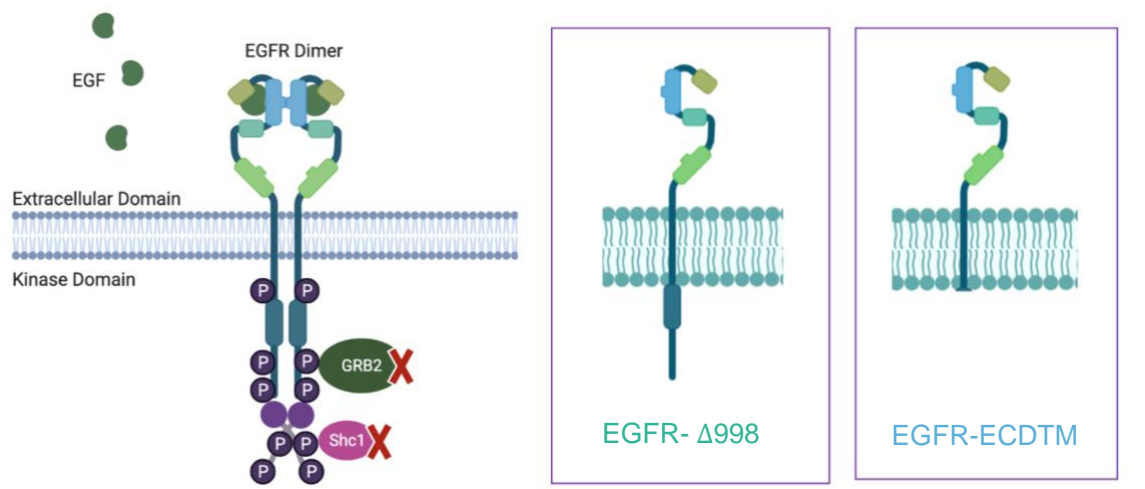


Figure 4. EGFR KO and Truncation Mutants. Left: EGFR's adaptor proteins Shc1 and Grb 2 that were knocked out of the cell. Right: Truncation mutants EGFR-Δ998 and EGFR-ECDTM.

Récepteur d'Origine Nantais (RON)

The Récepteur d'Origine Nantais (RON), also known as macrophage stimulating 1 receptor, is another member of the RTK family and belongs to the Met sub-family. Like EGFR, RON's discovery in the early 1990s⁴⁰ preceded the discovery of its ligand, macrophage-stimulation protein (MSP) in 1978.⁴¹ RON follows the signaling trends that are characteristic of the RTK family. Upon ligand binding, dimers form, leading to phosphorylation, or activation of the kinase domain, resulting in downstream signaling (as shown in **Figure 5**). RON is also highly expressed in cancerous tumors and is heavily involved in invasiveness.³ Little is known about the mechanisms of activation and downstream signaling related to RON but, crystallographic studies suggest that RON homodimers can be formed in the absence of its ligand.⁴²

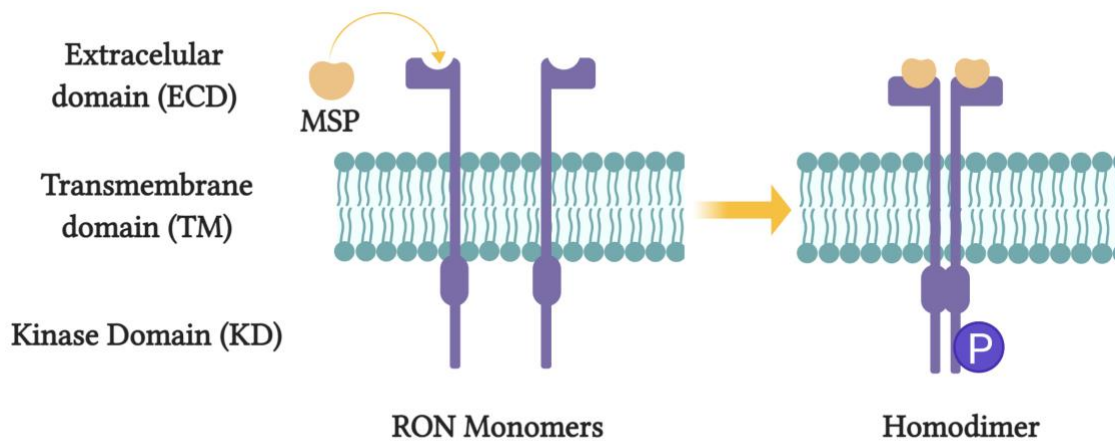


Figure 5. RON signaling overview. Upon ligand binding RON is thought to form a dimer that results in activation of the kinase domain which then leads to downstream signaling that will ultimately elicit a cellular response.

Although they were independently discovered and are structurally different, the combined expression of EGFR and RON has often led to a worse prognosis for cancer patients.³ This observation has raised questions about the potential cooperation, or crosstalk between the receptors and inspired studies that have delivered evidence of crosstalk between the two. The studies suggest that crosstalk between the receptors not only exists but, it may be a source of therapeutic resistance.^{3,43,44,45} The mechanisms by which crosstalk occurs are still under investigation but, biochemical evidence has shown that upon EGFR stimulation (with EGF), RON becomes phosphorylated, even in the absence of its ligand (MSP).⁴⁴ The observation suggests that there may be an underlying mechanism that is perpetuating the phosphorylation or activation of RON through EGFR. This study aims to further support the theory that EGFR can directly phosphorylate RON even in the absence of RON's ligand, MSP when RON and EGFR are co-expressed as shown in **Figure 6**. We quantified RON's dynamics by analyzing the changes in diffusion for a variety of conditions. A slowdown in RON mobility resulting from EGF stimulation would further support the theory that EGFR can directly phosphorylate RON.

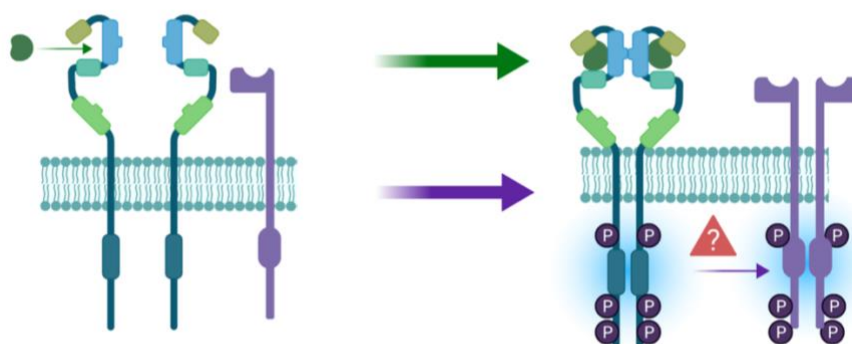


Figure 6. EGFR-RON Crosstalk. RON is activated and phosphorylated in the absence of its ligand MSP in the presence of EGF + EGFR indicating that EGFR-RON crosstalk may be responsible for RON phosphorylation. (Created with BioRender.com)

Fluorescence microscopy & Single-Particle Tracking (SPT)

Fluorescence microscopy has enabled the visualization of cellular components at micro and nanometric scales by capturing the illumination of specific targets down to single molecules. The ability to capture photons emitted from single fluorescing molecules (or tags) allows fluorescence microscopy to overcome barriers otherwise imposed by diffraction limits. In turn, this facilitates the study of single proteins such as EGFR and RON in a cellular environment.

A fluorescence microscope optic set-up like the one used in this study is shown in **Figure 7**. The set-up is comprised of a microscope with a specimen mount and light source (lamp or laser). The specimen containing a fluorophore of choice is mounted on the microscope. A light source emits light that passes through an excitation filter that selects a specific wavelength of light to pass through the sample and excite the fluorophore. Once the fluorophore has been excited, it emits light at a longer wavelength than the excitation wavelength due to the mechanism of fluorescence. The mechanism of fluorescence is a basic

principle outlining the following: when a particle (fluorophore) is excited, it absorbs high-energy photons that promote it to an excited state followed by a relaxation state. As the particle travels back to its ground state, energy dissipates, resulting in an emission of a photon of lower energy (or a longer wavelength). The difference in wavelengths allows for the separation of the emitted photons and excitation light. The emitted photons travel back through the objective and are directed by the dichroic mirror towards the emission filter. Once the emitted light is filtered, it is caught by a detector, captured by a camera, and then sent to the computer for processing. The result is an image or collection of images over time. At this stage, the camera must be programmed at a frame rate that is slow enough to allow for enough signal collection while being sufficiently rapid to capture protein dynamics.

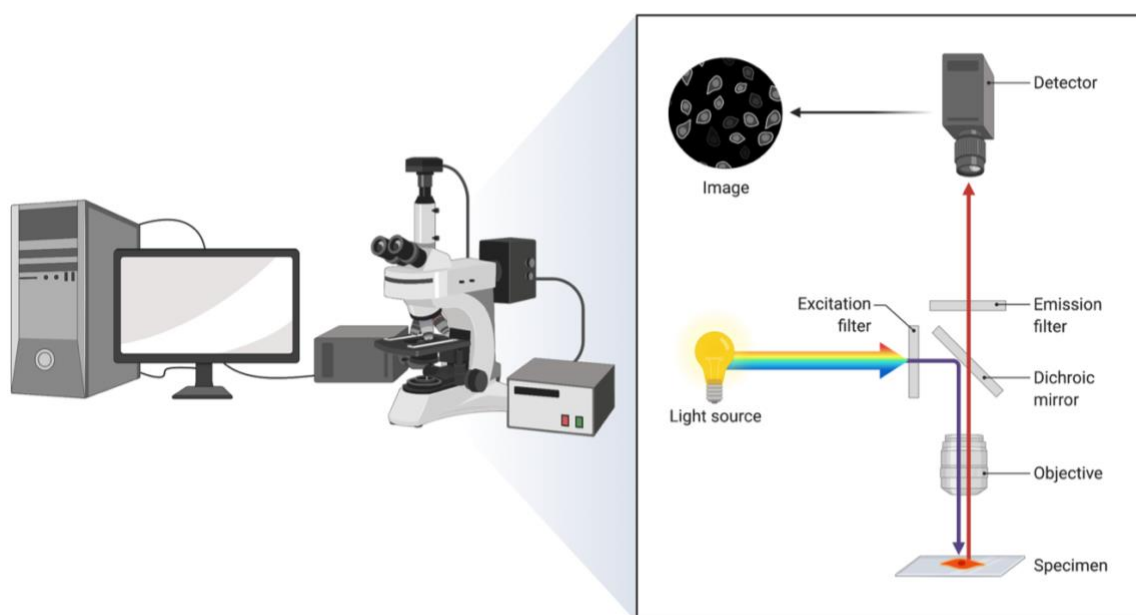


Figure 7. Schematic representation of the optical setup for SPT. The microscope has a mounting for the specimen and relies on a light source that goes through an excitation filter, followed by an objective and onto the specimen. As a result, light is emitted from the specimen, travels back through the objective and dichroic filter before going through an emission filter and into the detector. The light is then processed into an image by computer software. (Created with BioRender.com)

SPT is a specific fluorescence microscopy technique used to study single protein dynamics and interactions on a cell's plasma membrane.⁴⁶ The main advantage of SPT lies in its ability to capture the dynamics of fluorescent particles by taking advantage of high temporal and spatial resolution.⁴⁷ There are many fluorescent probes to choose from when performing SPT, including organic dyes, genetically expressed protein tags, fluorescent antibodies, and quantum dots (QDs). Many of these probes often lack stability or undergo photobleaching causing the imaging window to narrow. QDs are the exception. QDs are semiconductor nanoparticles composed of a semiconducting cadmium selenide core that is surrounded by a zinc sulfide exterior.⁴⁸ They usually have a coating that allows for attachment, or conjugation, of biologically active molecules allowing for highly specific targeting. On the imaging side, QDs provide a high signal-to-noise ratio, absorption cross-section, and quantum yield. Compared to their counterparts, QDs are highly selective and photostable for prolonged live-cell imaging,⁴⁹ making them an ideal imaging probe for this study. It is important to note that fluorophore labeling must be done at low densities for SPT to maintain differentiation between near proteins. Because the labeling density for this type of probe must be low, multiple cells must be imaged during each experiment to capture the heterogeneity of the proteins.

To capture the dynamics of the proteins using SPT, the proteins of interest were tagged with the QDs. Two different methods were imposed in this study and are shown in **Figure 8**. One involves using a hemagglutinin (HA)-tag on the N-terminus extracellular portion of the genetically modified proteins. The HA-tags were derived from the human influenza glycoprotein, hemagglutinin (HA)⁵⁰ and serve as a binding site for α -HA fab fragments that are attached to the QDs. QDs were coated with streptavidin and conjugated in house to biotinylated α -HA fab fragments. This allowed for indirect QD binding to the proteins.

Labeling the proteins with this method allowed us to capture the dynamics of the proteins in their resting, or unbound, state and in their activated, or bound, state when we used dark (non-fluorescent) EGF. The other method of labeling involved conjugating a streptavidin-coated QD to a biotinylated EGF ligand. This method allowed for the tracking of ligand-bound (activated/stimulated) proteins.

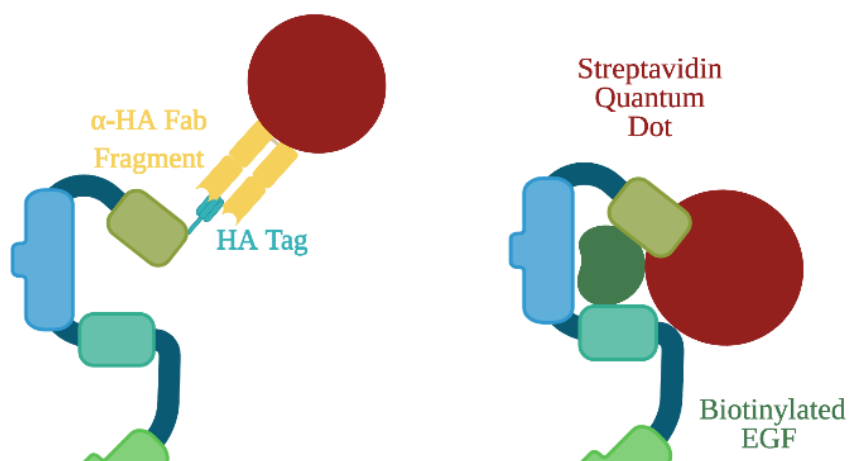


Figure 8. HA-EGFR QD labeling. Method one involves biotinylated α -HA fab fragment that binds to streptavidin coated QD (Left). Method two involves a streptavidin coated QD and biotinylated EGF (Right) (not to scale). (Created with BioRender.com)

Post imaging, SPT analysis was performed in MATLAB using scripts developed in-house. SPT analysis uses a 2-dimensional Gaussian estimate of the microscope's point spread function to fit, or localize, individual QDs. The code gives a coordinate estimate to each of the QDs captured during the imaging process. Once all the QD's are localized they get mapped or linked on a frame-by-frame basis (as shown in **Figure 9**) using probability estimates. The linking of mapped QDs from frame-to-frame results in QD paths traveled over time or trajectories.

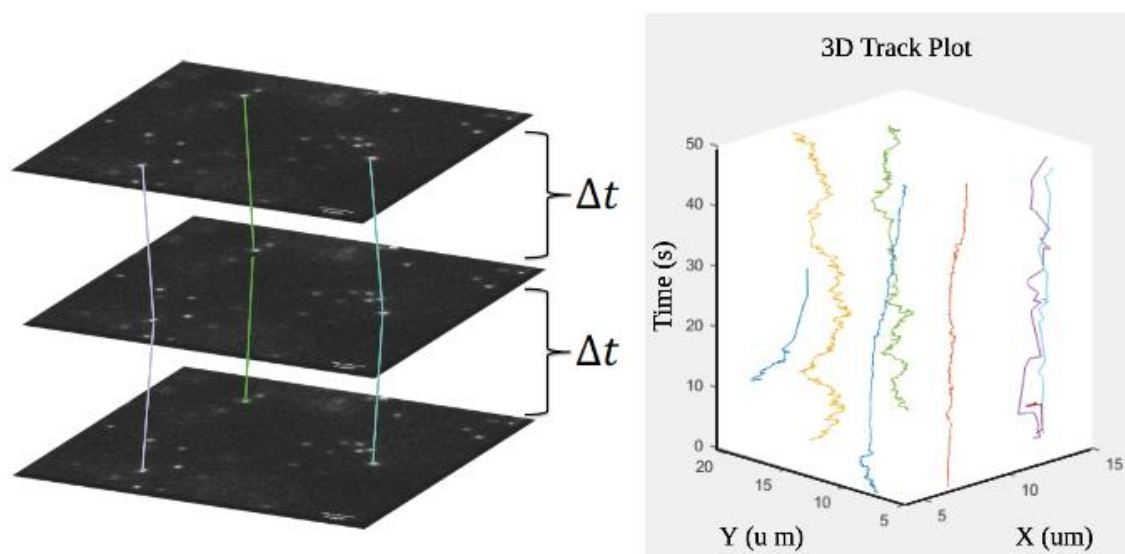


Figure 9. Schematic representation of trajectory formation. Frames collected over time are used to localize QDs on a frame-by-frame basis. The coordinates, or particle localizations are linked from frame to frame to create trajectories as shown on the left.

Mean Square Displacement (MSD) and Diffusion

We performed a mean-square displacement (MSD) fitting on the trajectories obtained using SPT to retrieve mobility readouts. MSD is the averaged square distances between a particle's start and end position $\langle r^2 \rangle$ for different time intervals (Δt) within a trajectory. The MSD fitting was performed using previously developed MATLAB® scripts. Once the MSD was fitted, we extracted the type of motion and the diffusion value associated with the proteins of interest. For this study, we mainly observed a straight slope with no curvature which is indicative of random, or Brownian, motion. The slopes of the MSD fittings were used to determine the diffusion coefficient, D . Diffusion values were later used for comparison between varying conditions.^{51,52} Diffusion provides information about a particle's mobility. A smaller diffusion coefficient (decreased slope) is associated with slower mobility. In

comparison, a larger diffusion coefficient (increased slope) would indicate more rapid mobility. It is important to note that for each condition, up to 120 cells were imaged and thousands of trajectories were analyzed before any conclusions were made.

HMM two color imaging analysis (dimerization measurement)

In simplified terms, Hidden Markov models (HMM) are tools used to recognize patterns. The model was originally developed for speech recognition⁵³ but, during the 90s, the model started being used to profile protein structures.⁵⁴ Today, the model is widely used and applied as an extension of this study to perform correlated motion quantification to confirm the formation of receptor complexes including RON:RON and EGFR:EGFR dimers. HMM is based on a Markov chain, a model that describes sequences of possible events based on the state of a preceding event. HMM assumes that the system is a Markov process with hidden states. A critical assumption for this process is that there is another observable process dependent on the hidden one. The observable process is used to better understand the hidden one through a set of mathematical equations derived by the Russian mathematician Andrey Markov and further outlined in the methods section.⁵⁵ In this study, we have a two-state HMM model where state one is indicative of a free protein, whereas state two is indicative of a protein in its dimer state.

Thesis scope and aims

As highlighted throughout this introduction, the complexity surrounding RTKs and their respective mechanisms has inspired many studies that aim to enhance our understanding of their structure and function. So far, the combination of biochemical and biophysical approaches has been instrumental in investigating and interpreting protein dynamics. Studies

that rely on the modern biophysical approach, SPT, have enabled diffusional dynamic measurements of RTK's that help to characterize receptor mobility. They have revealed an intriguing trend; a slowdown in mobility as a result of the stimulation.^{12,32,33,56} One of these studies postulated that "The slowed lateral motility of ligand-bound receptors is thus linked to tyrosine phosphorylation, possibly through protein scaffolding or signaling-induced changes in the local environment" (Low Nam).³³ Thus, it predicted that the mobility changes observed were a readout of EGFR signaling. This prediction inspired the first hypothesis of this study:

Hypothesis

Changes in receptor mobility that result from stimulation are correlated with receptor signaling.

Aims

Investigate the effects that limiting EGFR's signaling ability has on the receptor's mobility upon stimulation by quantifying changes in mobility that result from:

1. Removing adaptor proteins Shc1/Grb2
2. Removing all but one tyrosine binding site (EGFR- Δ 998)
3. Removing the entire kinase domain (EGFR-ECDTM)

As discussed in section 1.4, RTKs have been one of the main focuses of targeted therapies but, those therapies often lack the expected outcomes. One potential reason lies in their ability to undergo hetero interactions that could offer therapeutic escape routes. Understanding the mechanisms by which proteins collaborate or participate in crosstalk could uncover potential motives for therapeutic resistance. A recent study from our lab, currently under review, used biochemical and SPT approaches to study the crosstalk between EGFR and RON. We concluded that RON activation can result from EGF stimulation of cells that co-

express RON and endogenous EGFR.⁴⁴ The mechanism of crosstalk was not fully uncovered but, we investigated it in this study. We hypothesized the following:

Hypothesis:

EGFR directly phosphorylates RON regardless of RON's kinase activity.

Aims

1. Investigate the differences between mobility changes induced by EGF versus MSP stimulation.
2. Investigate the effects that inactivating RON's kinase domain (HA-RON-K1114M) has on RON's mobility upon EGF stimulation.
3. Investigate the effects that inhibiting EGFR's kinase domain has on RON's overall mobility

Like the previous studies, we used a combination of biochemical and biophysical approaches that were mentioned in sections 1.5 and 1.6 and are further described in Chapter 2.

CHAPTER 2

METHODS

Biochemical Methods

2.1.1 Cell lines and Reagents

HeLa wild-type and HeLa CCL2 Shc1/Grb2 KO cells were cultured in DMEM 1x (modified) with L-glutamine, supplemented with 10% fetal bovine serum (FBS; Thermo Fischer Scientific), 2 mM L-glutamine (Life Technologies), and penicillin/streptomycin (Life Technologies).

Chinese Hamster Ovary, CHOK1, cells were cultured in Ham's F-12 1x (modified) with L-glutamine, supplemented with 10% fetal bovine serum (FBS; Thermo Fischer Scientific), 2 mM L-glutamine (Life Technologies), and penicillin/streptomycin (Life Technologies).

Human epidermoid carcinoma A431 cells (ATCC, CRL-1555) were cultured in Dulbecco's Modified Eagle Medium (DMEM) supplemented with 10% HyClone cosmic calf serum (CCS; GE Healthcare Life Sciences), 2 mM L-glutamine (Life Technologies), and penicillin/streptomycin (Life Technologies).

Cell culture medium was from Caisson Labs, Biotinylated EGF was purchased from Invitrogen (Cat # E3477). Qdot 605 and Qdot 655 streptavidin conjugates were from Thermo Fisher Scientific (cat # Q10103MP and Q10123MP, respectively) and Afatinib (Cat #S1011) from Selleckchem. Recombinant human MSP and EGF were purchased from R&D Systems (Cat # 4306-MS and Cat # 236-EG respectively).

2.1.2 *HeLa CCL2 Shc1/Grb2 KO*

Dr. Cédric Cleyrat generated the HeLa CCL2 Shc1/Grb2 KO cell line in-house using CRISPR/Cas9 gene editing tools to knock out the two adaptor proteins from the cell. This is the first study to use this cell line.

2.1.3 *Plasmid cloning, cell transfections*

To establish cell lines stably expressing HA-EGFR-WT, EGFR-Δ998, or EGFR-ECDTM, CHOK1 parental cells were transfected with respective plasmids. The mutated EGFR truncation plasmids, lacking the C-terminal phosphorylation sites, or entire intracellular regions were generated by Dr. Steinkamp's lab by amplifying the truncated EGFR from pcDNA3.1-EGFR WT plasmid using standard PCR and cloning techniques. EGFR-Δ998 was truncated at amino acid 998 while ECDTM was truncated at amino acid 651. The transfections were performed by electroporation using the AMAXA Nucleofector System (Lonza). 5×10^6 CHOK1 cells were transfected with 8 μg of plasmid DNA using Nucleofection Solution V and program U-036. Transfected cells were selected for stable integration by growth in 1 mg/ml G418 (Caisson Labs) for 2 days, then sorted for HA-EGFR truncation mutant expression with a fluorescently conjugated α-HA antibody (α-HA AF-488) using an iCyt SY3200 cell sorter (Sony Biotechnology). Cells were allowed to recover and grow for 48 hours before performing experiments.

2.1.4 *Immunofluorescence staining*

CHOK1 cells containing the EGFR- FLWT or EGFR truncation mutants were plated onto glass coverslips. EGFR labelling was done in live cells with an α-HA-FITC fragment

antibody (α -HA AF-488) for 30 min in Tyrode's buffer (135 mM NaCl, 10 mM KCl, 0.4 mM MgCl₂, 1 mM CaCl₂, 10 mM HEPES, 20 mM glucose, 0.1% BSA, pH 7.2) on ice. Cells were treated with 10 nM EGF-AF647 on ice for 5 min, fixed in 4% PFA (200 μ l per chamber) for 15 min at RT, and washed with 10 mM Tris/PBS buffer. Samples were rinsed, incubated with DAPI, and mounted with Prolong Gold or Diamond (Thermo Fisher Scientific) overnight. Confocal images were acquired using a 63x/1.40 oil objective on a Zeiss LSM800 microscope.

2.1.5 Cell Sorting

Transfected CHOK1 cells were allowed to recover for 48 hours. Post-recovery, the cells were sorted for EGFR-FLWT (or EGFR mutants) expression by labeling with a fluorescently conjugated α -HA antibody (α -HA AF488) and using the iCyst SY3200 cell sorter from Sony Biotechnology. After sorting, the cells were placed in 1 mg/ml G418 (Casisson Labs) to retain more expressing cells.

2.1.6 Multiplex Immunoblotting

For western blotting, BCA protein assay kit (cat # 23235) was used along with primary antibodies EGFR- R&D (AF231 Gt), PY1068 (CST #2236 Ms), EGFR XP (CST 4267 Rb), PY1068 (CST #2236 Ms), RON (CST #2654 Rb) PY20 (SC #508 Ms), PY99 – (SC #7020 Ms). Secondary antibodies used were Donkey α -Goat 800, Donkey α -Mouse 680, Goat α -Rabbit 800 and Goat α -Mouse 680 (Thermo Fisher Scientific).

Whole lysates (20 μ g) or IP samples were boiled with reducing sample buffer, subject to SDS-PAGE, and transferred to nitrocellulose membranes using the iBlot2 system (Life Technologies). Membranes were blocked for 30 min in 3% BSA / 0.1% Tween-20 / TBS and

probed overnight with primary antibodies at 4°C. Membranes were incubated with IRDye fluorescent secondary antibodies for one hour at RT washed, and dual color detection was performed using the Odyssey Fc Imaging System (Li-Cor).

RON lysates required further purification by immunoprecipitation techniques. A BCA protein assay was performed to quantify the amount of protein per sample of condition to be analyzed and an equal amounts of protein per condition were prepared for the immunoprecipitation. 10 uL of α -HA magnetic beads (Cell Signaling Technology) were added to each condition and left to rotate over night at 4°C. Beads were washed with PBS-Tween (0.05%). Samples were then placed in magnet capture beads until the supernatant was completely clear, supernatant was removed, and this was repeated four times. After final wash, 25 ul of 2x reducing buffer was added and the gel was run as previously described.

Microscopy and mathematical methods

2.1.7 Microscope & camera set-up

Imaging was performed using an inverted widefield microscope (Olympus IX71) with a 60x 1.2 numerical aperture water objective as previously described by Valley *et al*, 2015.¹² A mercury lamp was used for excitation. Emitted light was filtered through a 625 nm dichroic filter and 600/20 nm, 655/40 nm emission filters that further split the emitted light onto two different quadrants of the electron-multiplying charge-coupled device (EMCCD) camera (iXon 897 Andor technologies). Images had a pixel size of 0.16 μ m and were acquired at a rate of 20 frames per second with a duration of 50 seconds for a total collection of 1,000 frames. Channel registration was implemented to distinguish between the different colored QDs and was performed by assigning quadrants of the EMCCD camera a distinct fluorescence emission channel. Fiducials for channel alignment were collected by illuminating a slide containing a

nanogrid (Miraloma Tech) composed of 20×20 array of 200 ± 50 nm holes, or bright spots, at an intrahole distance (nonregular) of 3 ± 1 microns (total size $\sim 60 \times 60$ microns). The grid provides an estimate of single point emitters that appear on both channels. Then, the intensity is optimized to maximize photons while avoiding saturation. Fiducials were collected before and after each round of imaging. The bright spots from the fiducials were then used as control points and the two channels were overlaid based on the registration of the spots. These were used to create a locally weighed mean transform matrix using MATLAB®. Image Processing Toolbox (The MathWorks, Inc.)™. The method selected was *fitgeotrans* parameter *n* set to 10. The transform was applied to coordinates from the raw data with another method called *transforPointsInverse*.

The remaining errors post correction procedure for the channel registration were calculated using the following equation. Where $(x_{1,i}, y_{1,i}, x_{2,i}, y_{2,i})$ were a set of control points for $i = 1, 2, \dots, NPairs$. The first subscript denotes channel and the second denotes the pair number. The locally weighted mean corrections are applied to the control points $(x_{1,i}^*, y_{1,i}^*)$.

$$\sigma_{overlay} = RSME = \sqrt{\frac{1}{NPairs} \sum_{i=1}^{NPairs} [(x_{1,i}^* - x_{2,i})^2 + (y_{1,i}^* - y_{2,i})^2]} \quad \text{Equation 1}$$

2.1.8 Live cell imaging

Cells were seeded in 8-well chamber slides (Nunc Lab-Tek) at a density of 20,000/well and allowed to adhere overnight and up to 48 hours. For treated HeLa cells, EGFR kinase activity was inhibited by pretreating with 10 μ M Afatinib for at least 15 min and maintained through the experiment. EGFR-FLWT, truncation mutants or RON proteins were tracked via QDs conjugated to biotinylated α -HA Fab fragments that bind to the N-terminus HA-tag or

via QDs conjugated to biotinylated EGF. CHOK1 cells were incubated with 200 pM α -HA-QDs or 400 pM EGF-QDs (605 or 655) for 1 min while A431 cells were incubated with α -HA-QDs for 5 min, at 37°C followed by 3x washes with Tyrode's buffer, to obtain single-molecule density on the apical surface. For α -HA-QD tracking plus non-fluorescent EGF, cells were treated with 25 μ M dark EGF for 30 sec and imaged. Physiological temperature (34 – 36°C) was maintained using an objective heater (Biopetechs). SPT was performed for up to 7 min per well (labeling was done one well at a time).

2.1.9 *Single-Particle Tracking (SPT)*

MATLAB® codes developed in house enabled SPT analysis. We used a 2-dimensional Gaussian point spread function model to estimate coordinates for the localization of bright spots in the raw images. The resulting emitter coordinates, or single-particle localizations were connected frame to frame to create particle trajectories. MATLAB® codes previously developed in-house facilitated the connection of broken tracks by comparing the position of all the particles found in a frame and estimating the probability that the same particle was in the next frame.

$$P(p_i \rightarrow p_{i+j}) = e^{-\frac{(x_i - x_{i+j})^2 + (y_i - y_{i+j})^2}{4D\Delta t}} \quad \text{Equation 2}$$

Where D is the diffusion coefficient, Δt the time between observations in frames $(i, i + j)$.³³

The estimated diffusion coefficient used was 0.02 $\mu\text{m}^2/\text{s}$. P-values and Δt are user defined, the P-value is determined by using an in-house script that allows for iterations that converge to the best P-value.

2.1.10 Mean Square Displacement (MSD)

Between 40 and 120 cells were imaged per condition, resulting in hundreds of trajectories. Mean squared displacement fittings of the trajectories were obtained as previously described using software developed in house^{12,33,57} in which $\Delta t = 1,2,3,4$ and 5 frames (not including 0). Diffusion values were obtained from the slope of the averaged MSD fittings for each of the analyzed conditions.

2.1.11 Hidden Markov Model (HMM)

HMM analysis requires a defined emission density for each model state. As described in *Nitta et al.*, emission density is the probability density of observing a separation given an underlying state of HMM. A two-state model developed previously could be used to characterize RON, EGFR and EGFR truncation mutants behavior. The model acknowledges two states: free and dimer. The emission density for the free state was found based on the previous observation. The density was denoted as $g(d_n|d_{n-1}, free)$ where d_n is the separation of two particles n and $n - 1$. Analogous densities in Cartesian coordinates were used for this analysis where the density was denoted as $f(\Delta x, \Delta y|free)$, where $\Delta x = \Delta x_n - \Delta x_{n-1}$ and $\Delta y = \Delta y_n - \Delta y_{n-1}$, $(\Delta x_n)^2 + (\Delta y_n)^2 = d_n^2$ and $(\Delta x_{n-1})^2 + (\Delta y_{n-1})^2 = d_{n-1}^2$. Quantities of Δx and Δy assumed to be normally distributed with mean zero and variance $\sigma_n^2 = \sigma_{1,n}^2 + \sigma_{2,n}^2 + \sigma_{1,n-1}^2 + \sigma_{1,n-2}^2 + 2(2D)\Delta t_n$ where $\sigma_{\frac{1}{2},n}$ is the standard error of the estimates of particle positions $\frac{1}{2}$ in observations $n/n-1$. D is the diffusion coefficient of each of the particles and $\Delta t_n \equiv t_n - t_{n-1}$ is the time between observations n and $n-1$. The additional multiple of 2 in front of the diffusion coefficient can be understood by deriving $f(\Delta x, \Delta y|free)$ and treating one of the particles as fixed. As a result, the moving particle must diffuse with twice its true

diffusion coefficient. The expression $f(\Delta x, \Delta y | free)$ is then converted to polar coordinates (d_n, θ) resulting in $g(d_n, \theta | d_{n-1}, free)$. The desired emission density $g(d_n | d_{n-1}, free)$ is then obtained by integrating $g(d_n, \theta | d_{n-1}, free)$ over θ assuming that θ is distributed uniformly on the interval $[0, 2\pi]$ and results in the expression below

$$g(d_n | d_{n-1}, free) = \frac{d_n}{\sigma^2} \exp\left(-\frac{d_n^2 + d_{n-1}^2}{\sigma_n^2}\right) I_0\left(\frac{d_n d_{n-1}}{\sigma_n^2}\right) \quad \text{Equation 3}$$

where I_0 is the zeroth order modified Bessel function of the first kind. The free state emission density for the first observation is estimated by the expression $g(d_1 | d_1, free)$ treating each appearance of d_1 as independent observations of the separation in subsequent frames (setting $\Delta t_n = 1$ frame).

A similar approach was used for the dimer state. First, we found the probability density $f(\Delta x, \Delta y | dimer)$ where Δx and Δy are now defined as $\Delta x \equiv \Delta x_n - \Delta x'$ and $\Delta y \equiv \Delta y_n - \Delta y'$ where $\Delta x'^2 + \Delta y'^2 = L_{dimer}^2$ with L_{dimer} being the true separation between fluorophores attached to the two receptors that make up a dimer. The terms Δx and Δy are treated as normally distributed random variables with mean 0 and $\sigma_n^2 = \sigma_{1,n}^2 + \sigma_{2,n}^2 + \sigma_{overlay}^2$. The addition of the constant term $\sigma_{overlay}^2$ in the variance is included as an approximation to the true effect of the channel registration error, which in reality complicates the derivation of $g(d_n | d_{n-1}, dimer)$ from $g(d_n, \theta | d_{n-1}, dimer)$ by breaking the assumption that θ is distributed uniformly on the interval $[0, 2\pi]$. The approximation has little consequence since the channel registration contribution $\sigma_{overlay}^2$ is typically an order of magnitude smaller than

the sum $\sigma_{1,n}^2 + \sigma_{2,n}^2$. Following the derivation of the free state emission density, the expression for the dimer state emission density is yielded:

$$g(d_n | L_{dimer}, dimer) = \frac{d_n}{\sigma_n^2} \exp\left(-\frac{d_n^2 + L_{dimer}^2}{\sigma_n^2}\right) I_0\left(\frac{d_n + L_{dimer}}{\sigma_n^2}\right) \quad \text{Equation 4}$$

2.1.12 Rate parameter estimation

The rate parameters are estimated by maximizing the likelihood of the observed data with respect to the rate parameters of the HMM.^{58,59} The likelihood of the HMM with a set of rate parameters θ given the observed data $d = [d_1, d_2, \dots, d_N]$ takes the form:

$$L(\theta | d) = \pi T_1 P_1 T_2 P_2 \dots T_N P_N \cdot (1, 1, 1)^T \quad \text{Equation 5}$$

Where $\pi = [g(d_1 | L_{dimer}, dimer), g(d_1 | d_1, free)]$, T_n for $n \in 1, 2, \dots, N$ is a 2x2 transition matrix whose elements give the transition probabilities for the interstate transitions of the HMM and P_n for $n \in 1, 2, \dots, N$ is a 2x2 diagonal matrix whose elements p_{11} and p_{22} give emission probability densities of an observation d_n given an underlying dimer state or free state. The elements $t_{i,j}$ for $i, j \in 1, 2$ of T_n are given by

$$t_{1,2} = 1 - \exp(-\Delta t_n k_{1,2}) \quad \text{Equation 6}$$

$$t_{2,1} = 1 - \exp(-\Delta t_n k_{2,1}) \quad \text{Equation 7}$$

$$t_{1,1} = 1 - \Delta t_{1,2} \quad \text{Equation 8}$$

$$t_{2,2} = 1 - \Delta t_{2,1} \quad \text{Equation 9}$$

where $k_{1,2}$ is the transition rate from the dimer state to the free state and $k_{2,1}$ is the transition rate from the free state to the dimer state. The rate parameters $k_{1,2}$ and $k_{2,1}$ are found by maximizing the sum of the log likelihoods over all candidate interactions $\sum_{interactions} \log L(\theta|d)$. The standard errors of the rate parameters estimates were estimated from elements $h_{i,i}$ of the Hessian of the negative log-likelihood H as $\sqrt{h_{i,i}^{-1}}$ where $i = 1$ corresponds to $k_{2,1}$ and $i = 2$ corresponds to $k_{1,2}$.

2.1.13 Statistical analysis

The MATLAB® programs that were developed for data analysis rely on integrated statistical analysis. The error bounds associated with the results are symmetrically computed with a 95% confidence interval and can be found in the database of results and as part of the legend in the MSD plots. An additional statistical analysis approach is used to determine whether the differences observed in diffusion values between conditions are statistically significant. MATLAB® saves a database with the diffusion values, and the respective errors that were calculated on a per movie (per cell) basis. Prior to averaging the diffusion coefficient results with a 95% confidence interval, the diffusion coefficient results were used to compare statistical significance pertaining to the differences between conditions. This was done using two-sample, two-tail t-test assuming unequal variances with $p < 0.05$.

CHAPTER 3

RESULTS AND DISCUSSION

Cell line generation & characterization

To study the effect that limiting EGFR's signaling ability would have on its observed mobility, I first generated cell lines expressing wild-type (WT) EGFR and the two EGFR truncated mutants EGFR- Δ 998 and EGFR-ECDTM shown in **Figure 10**. The creation, stabilization, and characterization of cell lines containing EGFR-WT and the truncation mutants were preferred over utilizing transiently transfected cell lines. Transiently transfected cell lines would require a transfection followed by a 48-hour recovery period prior to each experiment. Stable cell line generation was a simpler approach in the long run that provided consistency between experiments. Chinese hamster ovary (CHOK1) cells were selected as the host of the plasmids because they do not express native EGFR, making them excellent for control purposes. Post transfection, the cells were allowed to recover and then sorted and checked for expression as previously described in the Methods sections 2.3 and 2.4.



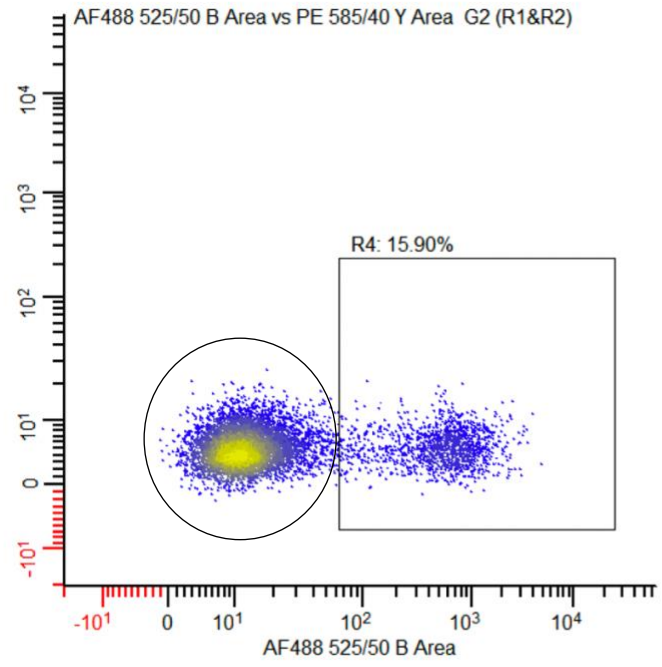
Figure 10. EGFR & EGFR mutant cartoon. Left is a depiction of the EGFR full length wild-type, middle shows EGFR- Δ 998 construct that is missing the C-terminal phosphorylation tail

and right is the extracellular transmembrane domain construct that is missing the entire kinase domain. (Created with BioRender.com)

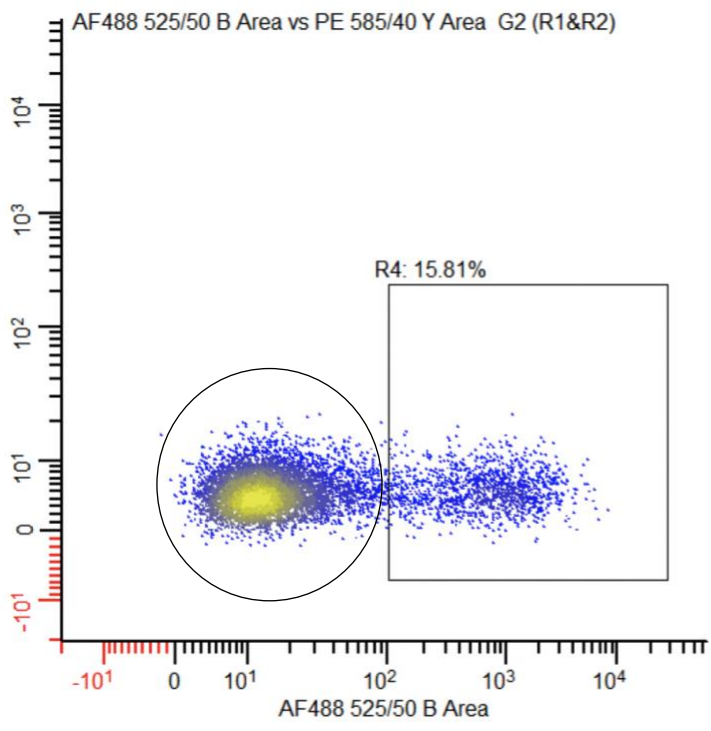
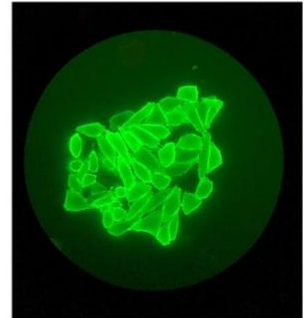
After allowing the cells to recover from the transfection, they were labeled and sorted. Note, each of the three proteins has a hemagglutinin (HA) tag at the N-terminus of their extracellular region. Therefore, they were all labeled with the fluorescently conjugated α -HA antibody (α -HA-AF488). Because the antibody is a specific target for α -HA, we can assume that the labeled cells were positively expressing the proteins of interest. When passing through the flow sorter, each cell's intensity of fluorescence was measured. The three-side scatter versus intensity plots shown in **Figure 11** display the results of the cell sorts. Only the cells with a measured intensity that fell within the selected range of acceptance (represented by a black box on the graph) were kept by the cell sorter. In technical terms, this action is called gating. The blue dots that lie outside of the box (encircled) represent the cells that did not meet the intensity of fluorescence requirement and were discarded by the sorter. Those cells were likely not expressing the protein. The yellow spot indicates where the highest density of cells fell in terms of fluorescence measurement. Most of the EGFR-WT and the two truncation mutants fell outside of the acceptable threshold, or gate, and were thus sorted out. For each of the conditions, less than half of the sorted cells were positively expressing their respective mutant but, enough cells were recovered to generate stable cell lines. Post-sorting, the cells were allowed to recover for another 48 hours while maintained in 1 mg/ml of G418, a selective agent used to increase the retention of expressing cells.

Once the cells recovered, immunofluorescent labeling techniques further verified expression. The three cell lines were labeled on ice using α -HA AF488, fixed, and mounted on a glass slide. The cells were imaged using a confocal microscope to check for fluorescence.

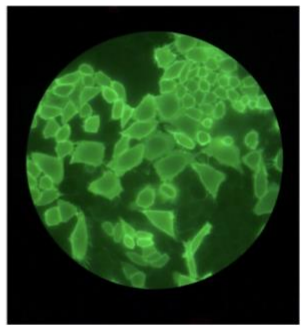
The image results are also shown in **Figure 11** (right). The green ring on the membrane of the cells confirms the presence of the α -HA-AF488 antibody. Recall that the α -HA-AF488 adheres to the HA tag on the N-terminus of the cell. Therefore, the green ring indicates that the plasmid is expressed on the cell's membrane.



EGFR-WT



EGFR Δ 998



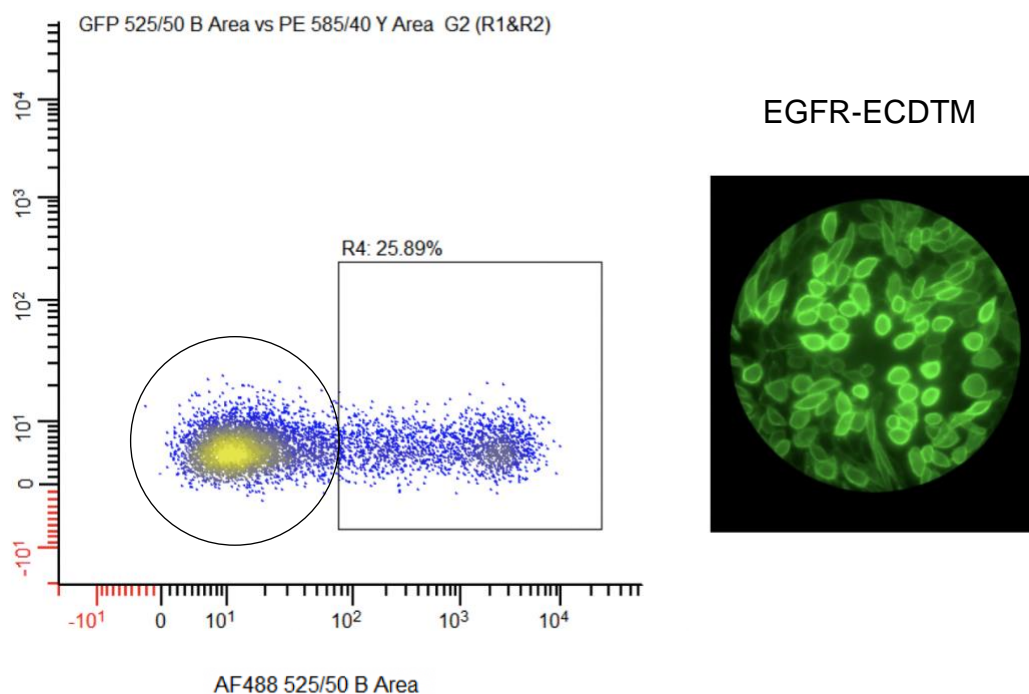


Figure 11. Cell line sorting and immunofluorescence results for expression verification. Left: Side Scatter vs. Intensity plots for α -HA antibody (α -HA-AF488) labeled cells. Cell's intensity of fluorescence was measured, and cells were selected based on a pre-determined range of fluorescence intensity. Blue dots represent individual cells, black box encompasses cells that were selected by the flow sorter. The cells on the left of the black box (encircled) represent the cells that did not meet the required intensity and were not selected by the flow sorter. Right: immunofluorescence results of each cell line. The fluorescent green ring on the cell's membrane indicates the proper trafficking of the EGFR variant to the cell membrane.

The final expression check was done using well-established western blotting (WB) methods. The WB results (shown in **Figure 12**) revealed details about the EGFR-WT and truncation mutant's presence, respective size, and response to EGF stimulation. The green bands confirmed the presence of EGFR and the truncation mutants. Western blotting uses electrophoresis to separate the proteins by size. The further up a band lies on a blot, the larger the protein pertaining to that band is. In this case, EGFR-WT is found at the top, indicating that it is the largest. It is followed by EGFR- Δ 998 (2nd largest) and EGFR-ECDTM (smallest).

This result is consistent with our expectations because EGFR- Δ 998 is smaller than EGFR-FLWT since it is missing the C-terminal tail of the cytoplasmic domain, while EGFR-ECDTM is not only missing the C-terminal tail but the entire intracellular region. In addition to the size verification, we were able to confirm that the EGFR-WT has the expected activation response to EGF stimulation. This is represented by a red band around the 170 kD line that is indicative of phosphorylation at tyrosine residue 1068 of EGFR. EGFR-WT is the only protein expected to have such a response because the two truncated mutants are missing the C-terminal tail that is necessary for phosphorylation. The absence of red bands under the EGF stimulated conditions verifies the lack of phosphorylation in the truncated mutants.

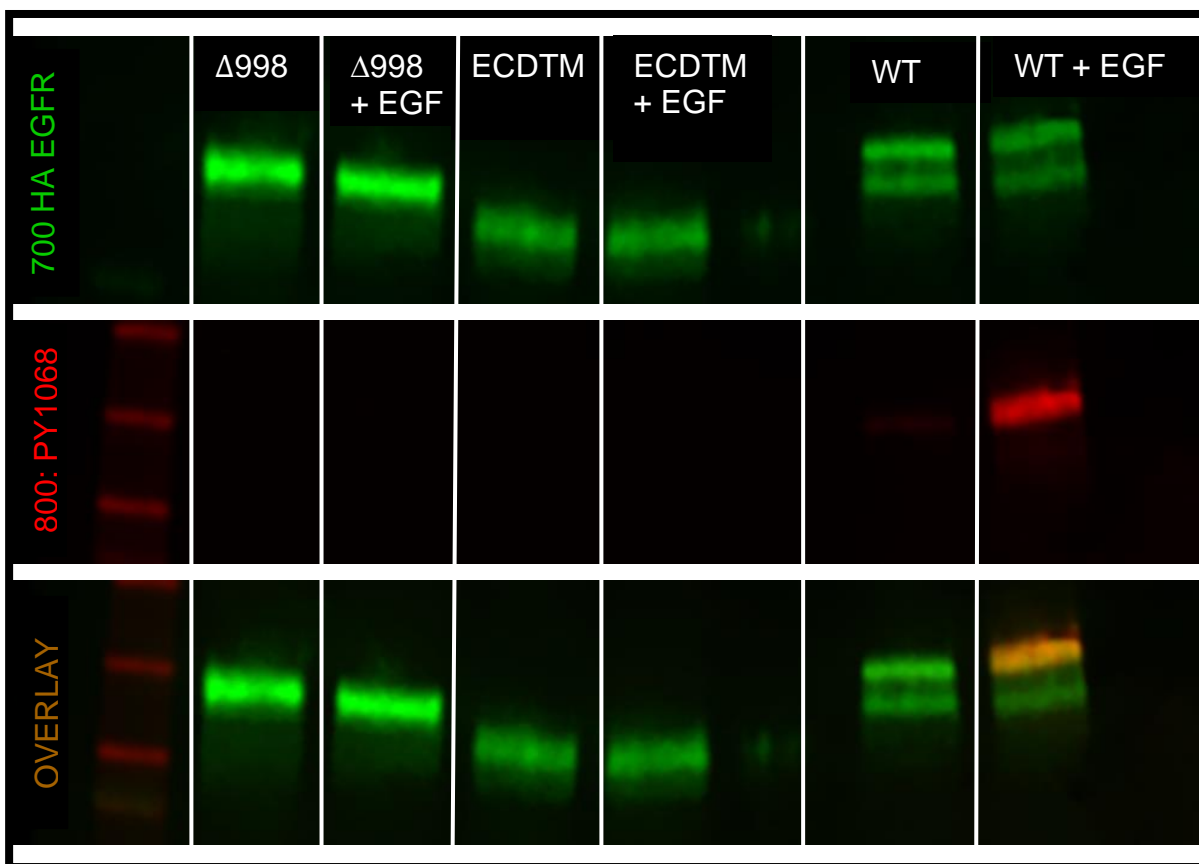


Figure 12. EGFR-WT, EGFR- Δ 998 and EGFR-ECDTM immunoblots. Blots for α -HA (green) and EGFR-PY1068 (red). Top blot (green) bands represent total protein for either EGFR-WT or truncation mutants. Their position along the y-axis indicates their respective

size. Larger proteins are found higher up while smaller proteins are found lower. The middle blot (red) band represents phosphorylation of the protein of truncation mutants. Only EGFR-WT + EGF was phosphorylated, as expected. Bottom blot is an overlay of the two channels and the orange band represents both, the presence, and phosphorylation of EGFR-WT.

Overview of SPT data presentation

We performed SPT using custom MATLAB® analysis as described in Chapters 1 and 2. The results are shown in two alternative ways, a dot plot (also known as a Beeswarm plot) and an MSD plot. The same data was used to generate both plots but, both are shown for comparison purposes. The horizontal bar on the Beeswarm plot is the average diffusion value that was calculated from the distribution of diffusion coefficients for that specific condition. One can find the conditions on the x-axis and the diffusion values on the y-axis in units of $\mu\text{m}^2/\text{s}$. The MSD plots, on the other hand, consist of ensemble MSD curves for each of the conditions along with a fitting applied at small Δt . The fitting allowed us to extract the slope or diffusion coefficient for each condition. The Δt can be found on the x-axis and the MSD value can be found on the y-axis with units of μm^2 . The legend displays the conditions along with the calculated diffusion values and the errors associated with each. All bar graphs present the diffusion coefficient as calculated from the fitting of the ensemble MSD with a 95% confidence interval.

Role of adaptor proteins in EGFR's mobility: Grb2 & Shc1

As previously described, Shc1 and Grb2 are examples of adaptor proteins recruited to phosphotyrosine residues on EGFR's C-terminal tail to initiate a downstream signaling cascade. **Figure 13** shows a simple recap of the Grb2 recruitment, that will lead to the formation of a multi-protein signaling complex and the initiation of downstream signaling.

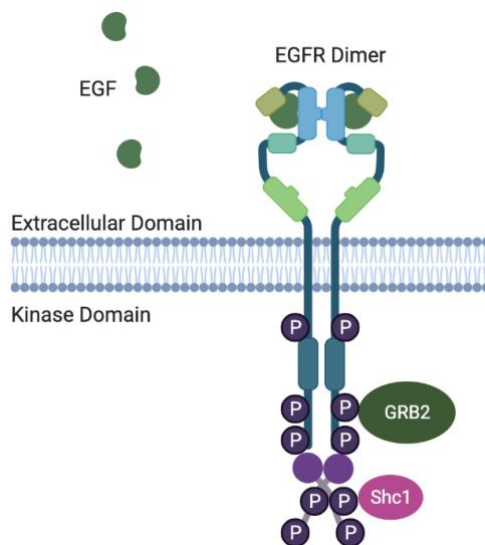


Figure 13. Overview of Shc1 & Grb2 protein recruitment post-dimerization. After dimerization, transphosphorylation of the C-terminal tail occurs and is followed by protein recruitment. This figure shows the recruitment of Shc1 & Grb2 that will then recruit other proteins to form a complex that'll result in a downstream signal that will elicit a cellular response. (Created with Biorender.com)

To quantify the effect that two adaptor proteins can have on EGFR's observed mobility changes, we looked at EGFR in HeLa and Shc1/Grb2 knock-out (HeLa-KO) cells. Unlike CHOK1 cells, HeLa cells contain endogenous EGFR. Thus, the EGFR found in these cells does not possess the HA-tag that enables indirect labeling. Instead, the EGFR found on these cells requires direct labeling for SPT (Shown in **Figure 14**. The direct labeling was done using QD655-EGF, which activates the protein. Therefore, we used an EGFR inhibitor, Afatinib, to inhibit the protein's kinase activity. By inhibiting the kinase activity, we were mimicking the protein's inactive or resting state since the Afatinib inhibitor would prevent Shc1 and Grb2 and other adaptor proteins from binding.

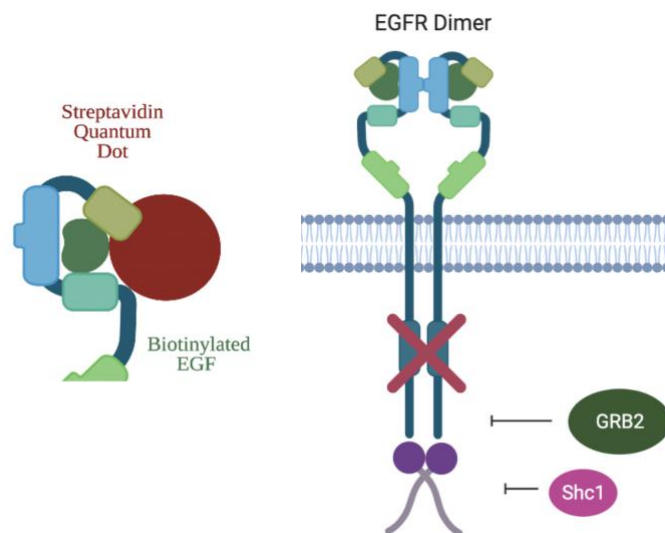
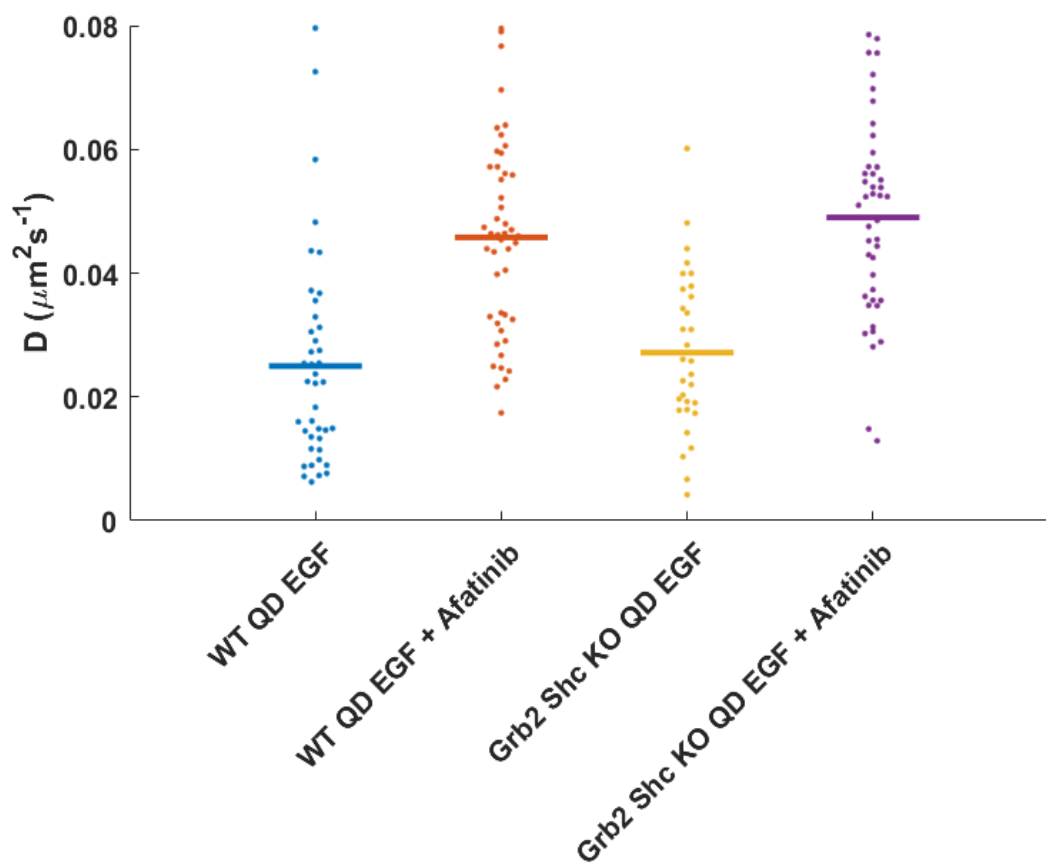


Figure 14. Direct QD binding of EGFR & EGFR's kinase domain inhibition. EGFR was directly labeled using QD655-EGF (left). To mimic the resting state of the protein, EGFR's kinase domain was inhibited with Afatinib which is represented as an X on the figure to the right. (Created with BioRender.com)

We performed SPT on the WT and KO cells using QD655-EGF with and without a 10 nM Afatinib treatment (an EGFR kinase inhibitor). As shown in the summary of results found in **Table 1** and **Figures 15** and **16**, the averaged diffusion of EGFR from HeLa cells decreased $\approx 48\% \pm 0.0039 \mu\text{m}^2/\text{s}$ when compared to its inhibited form. The EGFR found in the HeLa-KO cells decreased $\approx 42\% \pm 0.005 \mu\text{m}^2/\text{s}$ when compared to its own inhibited form. This observation indicates that EGFR from both cell lines experienced increased mobility when its kinase domain was inhibited. In other words, the ligand-bound uninhibited EGFR has slower mobility than the inhibited form.

A two-sample t-test assuming unequal variances ($p < 0.05$) revealed that even in the absence of Shc1 and Grb2, there is a significant decrease in mobility when EGFR's kinase domain is not inhibited and is stimulated with QD655-EGF. Although the average EGFR diffusional decrease from HeLa-KO cells seems to be less than the HeLa-WT ($\approx 6\%$), the

difference between the two is not statistically significant. Knocking out Shc1 and Grb2 did not have a significant effect on mobility (diffusional slowdown).



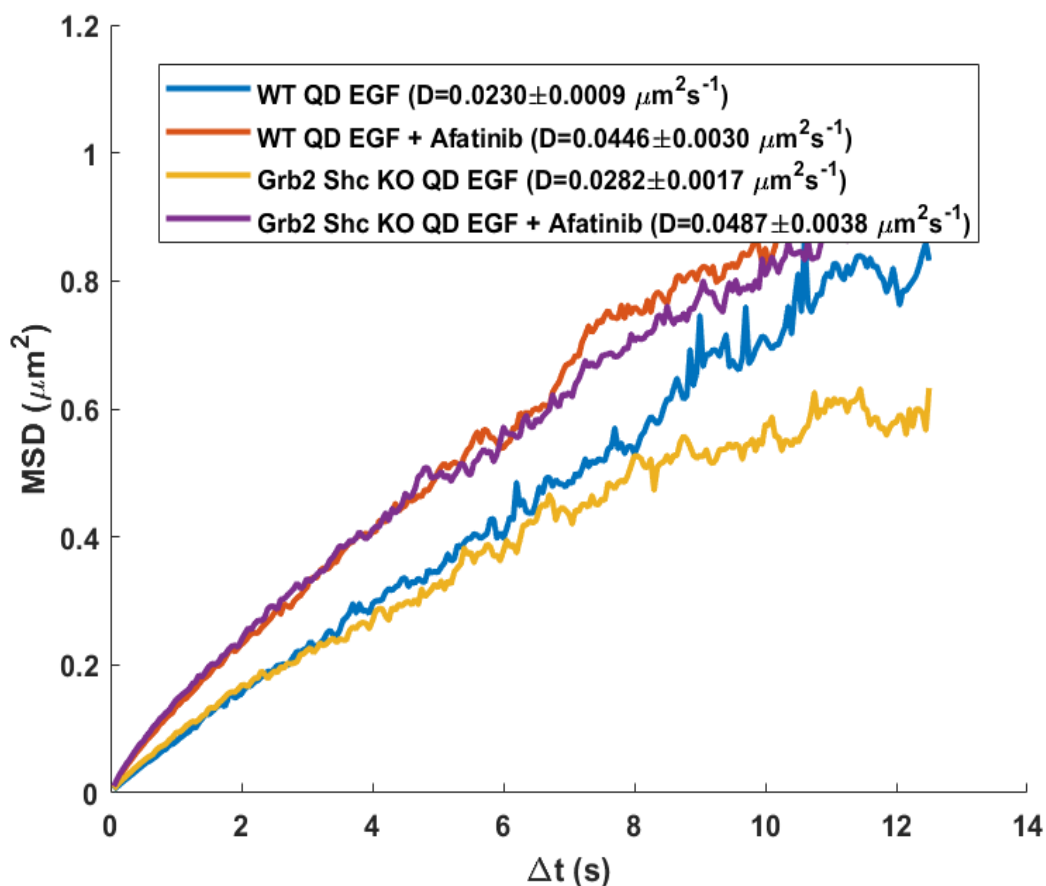


Figure 15. Plots comparing HeLa EGFR WT & Shc1/Grb2 KO \pm 10 μm Afatinib SPT results overview Top: Beeswarm Plot displays each cell's diffusion coefficient result in the form of a dot and the averaged value as a horizontal bar. Bottom MSD plot displays ensemble mean squared displacement for where a decrease in slope indicative of slower mobility. Results were plotted for 43 HeLa EGFR WT cells, 48 HeLa EGFR WT + Afatinib cells, 32 HeLa KO cells and 43 KO + Afatinib cells.

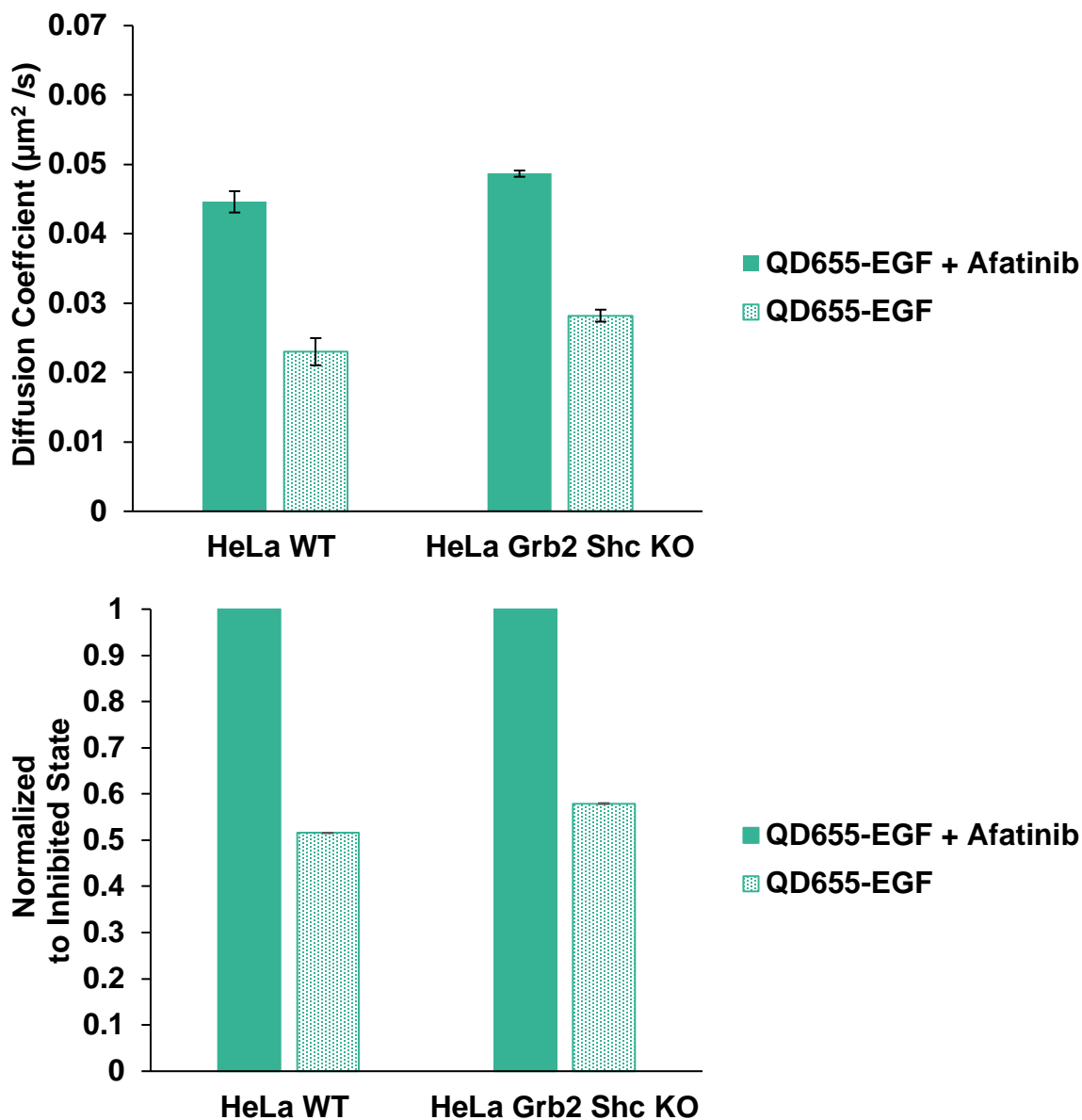


Figure 16. Diffusion coefficients for SPT of HeLa WT & Grb2/Shc1 KO QD655-EGF \pm 10 μm Afatinib. Top: bar graph displays the diffusion coefficient of inhibited and non inhibited EGFR. Bottom: bar graph displays the normalized values to the inhibited state of the EGFR \pm QD655-EGF. There is an statistically significant decrease in diffusion when EGFR is stimulated with QD655-EGF in its noninhibited form observed in both WT and KO cells. Diffusion coefficients are from the fit of the ensemble MSD plots and werror bars indicate 95% confidence interval.

Table 1. Results summary for HeLa WT and Shc1/Grb2 KO QD655-EGF \pm Afatinib. The difference in mobility between the inhibited to non-inhibited states of EGFR in both cell lines were statistically significant. When comparing the difference in EGFR mobility between the WT and KO cells, the results showed they were not statistically significant.

Variable 1	Average diffusion ($\mu\text{m}^2/\text{s}$)	Error (\pm)	Variable 2	Averaged Diffusion ($\mu\text{m}^2/\text{s}$)	Error (\pm)	Difference ($\mu\text{m}^2/\text{s}$)	Error (\pm)	% Decrease	P value (2-tail)	Significant
HeLa WT + Afatinib	0.0446	0.003	HeLa WT	0.023	0.0009	0.0216	0.0039	48%	5E-08	✓
HeLa CCL2 Shc1 Grb2 KO + Afatinib	0.0487	0.0038	HeLa CCL2 Shc KO	0.0282	0.0017	0.0205	0.0055	42%	9E-09	✓
HeLa WT	0.023	0.0009	HeLa CCL2 Shc KO	0.0282	0.0017	-0.0052	0.0026	-23%	0.5358	X

EGFR truncation mutants' contribution to EGFR mobility

As previously mentioned, our goal was to determine whether a decrease in diffusion (or mobility) was a readout of the proteins signaling. This set of experiments took the study one step further by allowing us to analyze the effects that resulted from further preventing the protein's signaling by using EGFR-WT (control) and EGFR truncation mutants EGFR- Δ 998 and EGFR-ECDTM (shown previously in **Figure 10**). Shc1 and Grb2 are not the only proteins that bind EGFR. Therefore, to make a fair assessment of the effect that adaptor proteins have on EGFR's mobility, we would need to knock out all the adaptor proteins. Doing so would pose two main issues, the first being that a cell cannot survive the knockout of multiple key proteins that play a variety of roles in survival. Second, even if the cells were to survive such a dramatic alteration, there is no guarantee that all adaptor proteins would be knocked out as there may be adaptor proteins that we have not identified. We worked around these concerns by changing our approach. Instead of attempting to figure out a way to account for all adaptor proteins, we simply removed EGFR's ability to recruit proteins. The EGFR- Δ 998 truncated mutant, or construct, is the version of EGFR without the C-terminal tail, meaning that it lacks the majority of phosphotyrosine sites. Although this truncation mutant has part of its kinase

domain, it is incapable of recruiting adaptor proteins. The EGFR-ECDTM mutant lacks the entire intracellular kinase domain and is also incapable of recruiting adaptor proteins. Studying these mutants in combination and comparing them to EGFR-WT could reveal which parts of EGFR critical for the slowdown observed upon EGF stimulation.

The cells containing HA-EGFR-WT, HA-EGFR- Δ 998, or HA-EGFR-ECDTM were tracked using either α -HA Fab fragments coupled to QDs (QD655-HA) in the presence or absence of saturating levels (25 nM) of dark EGF or using single-molecule levels of QD655-EGF. Post analysis, we created the MSD, Beeswarm, and bar plots shown in **Figures 17, 18, and 19**, and the results with statistical analysis results are shown in **Table 2**.

We found that upon stimulation with either 25 nM dark EGF or 400 pM QD655-EGF, EGFR-WT mobility was reduced, as expected. The diffusion coefficient decreased by $0.014 \pm 0.0027 \mu\text{m}^2/\text{s}$ and $0.0143 \pm 0.0027 \mu\text{m}^2/\text{s}$ respectively. This translates to $\approx 40\%$ decrease in mobility that is statistically significant according to a t-test of unequal variances ($p < 0.05$). This change is consistent with previous work from the Lidke Lab.^{12,33}

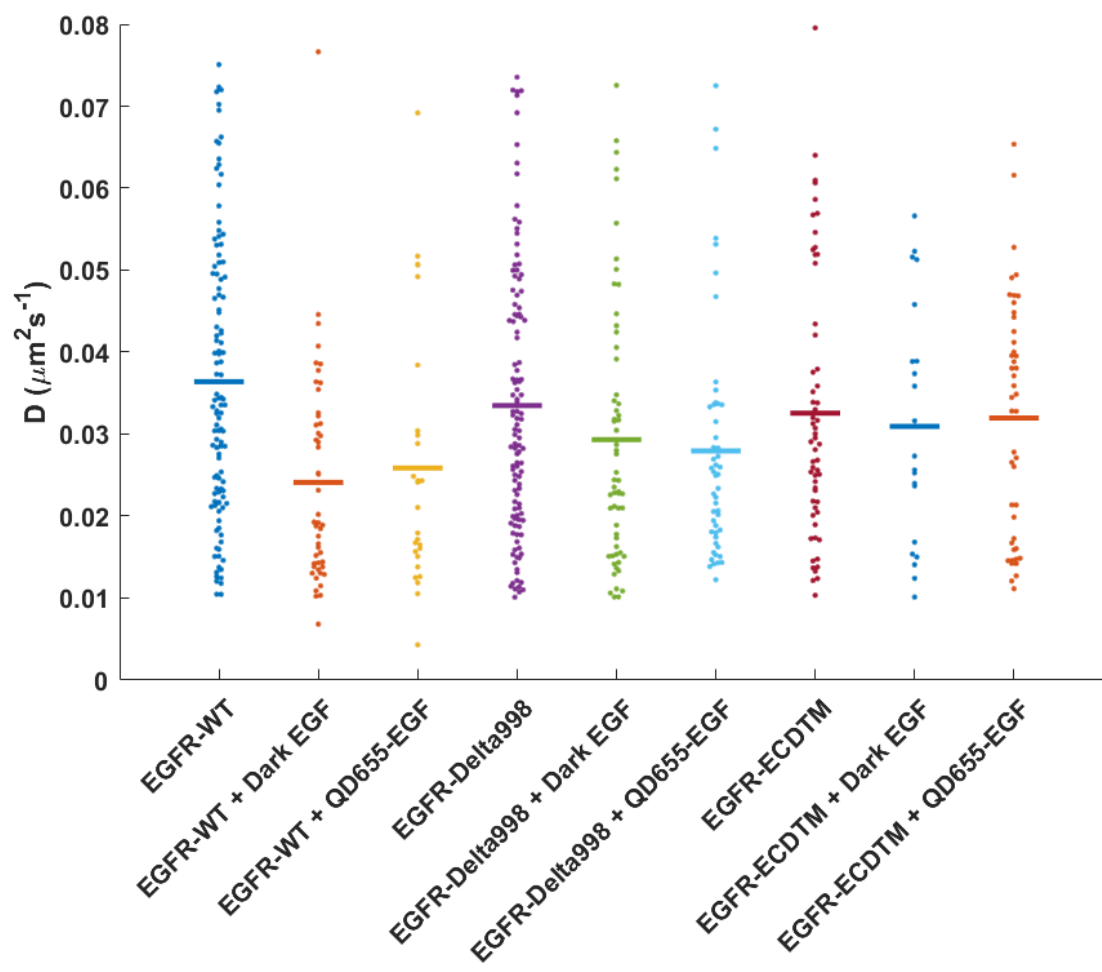
Figures 17, 18, and 19 also show the results for the EGFR- Δ 998 after identical stimulation. In this case, the diffusion coefficient of the EGFR- Δ 998 mutant decreased by $0.0043 \pm 0.0027 \mu\text{m}^2/\text{s}$ with 25 nM dark EGF and by $0.006 \pm 0.031 \mu\text{m}^2/\text{s}$ with 400 pM QD655-EGF equivalent to a respective $\approx 13\%$ and $\approx 18\%$ mobility decrease. A t-test of unequal variances ($p < 0.05$) revealed that the mobility decrease was statistically significant for dark EGF and Q655-EGF. The mobility decrease of EGFR- Δ 998 was significantly less than the slowdown that was observed for EGFR-WT.

Finally, upon dark 25 nM EGF stimulation, EGFR-ECDTM diffusion decreased by $0.005 \pm 0.0036 \mu\text{m}^2/\text{s}$ or $\approx 5\%$. Similarly, the diffusion decreased by $0.0025 \pm 0.0035 \mu\text{m}^2/\text{s}$ or

≈ 8% with QD655-EGF. Again, a t-test was performed but, this time it revealed that the decrease in mobility for EGFR-ECDTM upon EGF addition was not statistically significant.

We saw that phosphorylation of EGFR's C-terminal tail must be present to elicit a significant and prominent mobility decrease. The mobility decrease observed for the EGFR-Δ998 mutant was not as prominent as the decrease that was observed in the EGFR-WT upon EGF stimulation. Furthermore, the EGFR-ECDTM truncation mutant had an insignificant slowdown.

Considering what we know about the structure of the EGFR in dimerization terms, the extracellular, or ectodomain, is composed of four subdomains that undergo structural rearrangement to create a pocket for EGF binding and is followed by the exposure of a dimerization arm. EGFR-Δ998 and EGFR-ECDTM mutations still possess the key elements that EGFR relies on for dimerization but, we failed to see a mobility slowdown upon EGF stimulation that can compare to the one observed for EGFR-WT for both truncation mutants. This observation hints that dimerization might only be responsible for a portion of the observed decrease in mobility but, signaling ability must be present to observe the “full slowdown”. This observation would indicate that the receptor mobility measurements we are making are mainly a readout for receptor signaling and not simply indicative of dimerization. The events that occur post dimerization seem to weigh more heavily on the mobility decrease when compared to mobility decrease due to dimerization. The combined results support the hypothesis^{12,33} that changes in receptor mobility that result from stimulation correlate with receptor signaling.



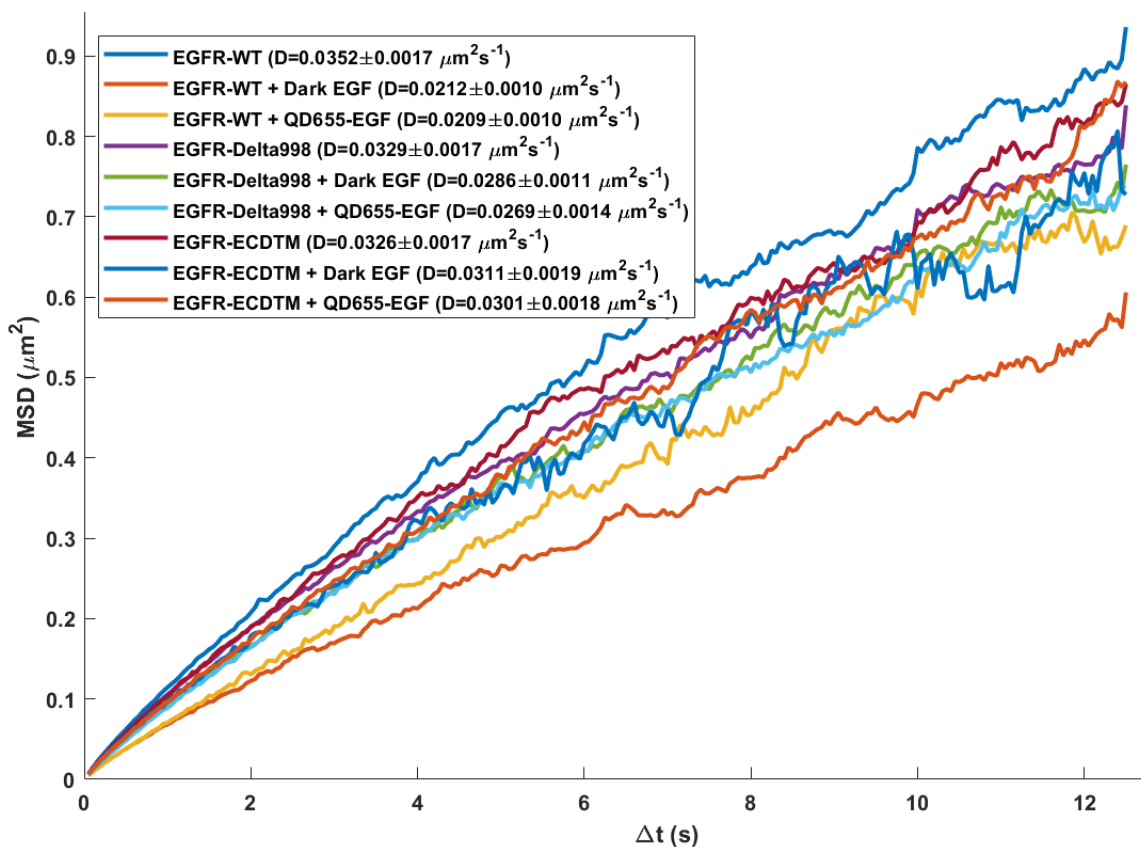


Figure 17. Plots comparing QD655- α -HA: HA-EGFR-WT, HA-EGFR- Δ 998 & HA-EGFR-ECDTM \pm Dark EGF or QD655-EGF. SPT results overview Top: Beeswarm Plot displays each cell's diffusion coefficient result in the form of a dot and the averaged value as a horizontal bar. Bottom MSD plot displays ensemble mean squared displacement where a decrease in slope is indicative of slower mobility. Results were plotted for 114 EGFR-WT cells, 49 EGFR-WT + dark EGF cells, 28 EGFR-WT + QD655-EGF cells, 117 EGFR- Δ 998 cells, 60 EGFR- Δ 998 + dark EGF cells, 51 EGFR- Δ 998 + QD655-EGF cells, 61 EGFR-ECDTM cells, 22 EGFR-ECDTM + dark EGF cells, 46 EGFR-ECDTM + QD655-EGF cells.

Table 2. Results summary for QD655- α -HA: HA-EGFR-WT, HA-EGFR- Δ 998 & HA-EGFR-ECDTM \pm Dark EGF or QD655-EGF or 400 pM QD655-EGF including errors and statistical analysis. The difference in mobility between EGFR-WT and Dark or QD655-EGF were both statistically significant as was the case for EGFR- Δ 998. The difference in EGFR-ECDTM mobility upon EGF stimulation was not significant.

Variable 1	Diffusion ($\mu\text{m}^2/\text{s}$)	Error (\pm)	Variable 2	Diffusion ($\mu\text{m}^2/\text{s}$)	Error (\pm)	Difference ($\mu\text{m}^2/\text{s}$)	Error (\pm)	% Decrease	P value (2-tail)	Significant
EGFR-WT	0.0352	0.0017	EGFR-WT + Dark EGF	0.0212	0.001	0.014	0.0027	40%	1.96E-06	✓
EGFR-WT	0.0352	0.0017	EGFR-WT + QD605-EGF	0.0209	0.001	0.0143	0.0027	41%	0.003982	✓
EGFR- Δ 998	0.0329	0.0017	EGFR- Δ 998 + Dark EGF	0.0286	0.001	0.0043	0.0027	13%	0.001588	✓
EGFR- Δ 998	0.0329	0.0017	EGFR- Δ 998 + QD605-EGF	0.0269	0.0014	0.006	0.0031	18%	0.027713	✓
EGFR-ECDTM	0.0326	0.0017	EGFR-ECDTM + Dark EGF	0.0311	0.0019	0.0015	0.0036	5%	0.660024	X
EGFR-ECDTM	0.0326	0.0017	EGFR-ECDTM + QD605 EGF	0.0301	0.0018	0.0025	0.0035	8%	0.82685	X

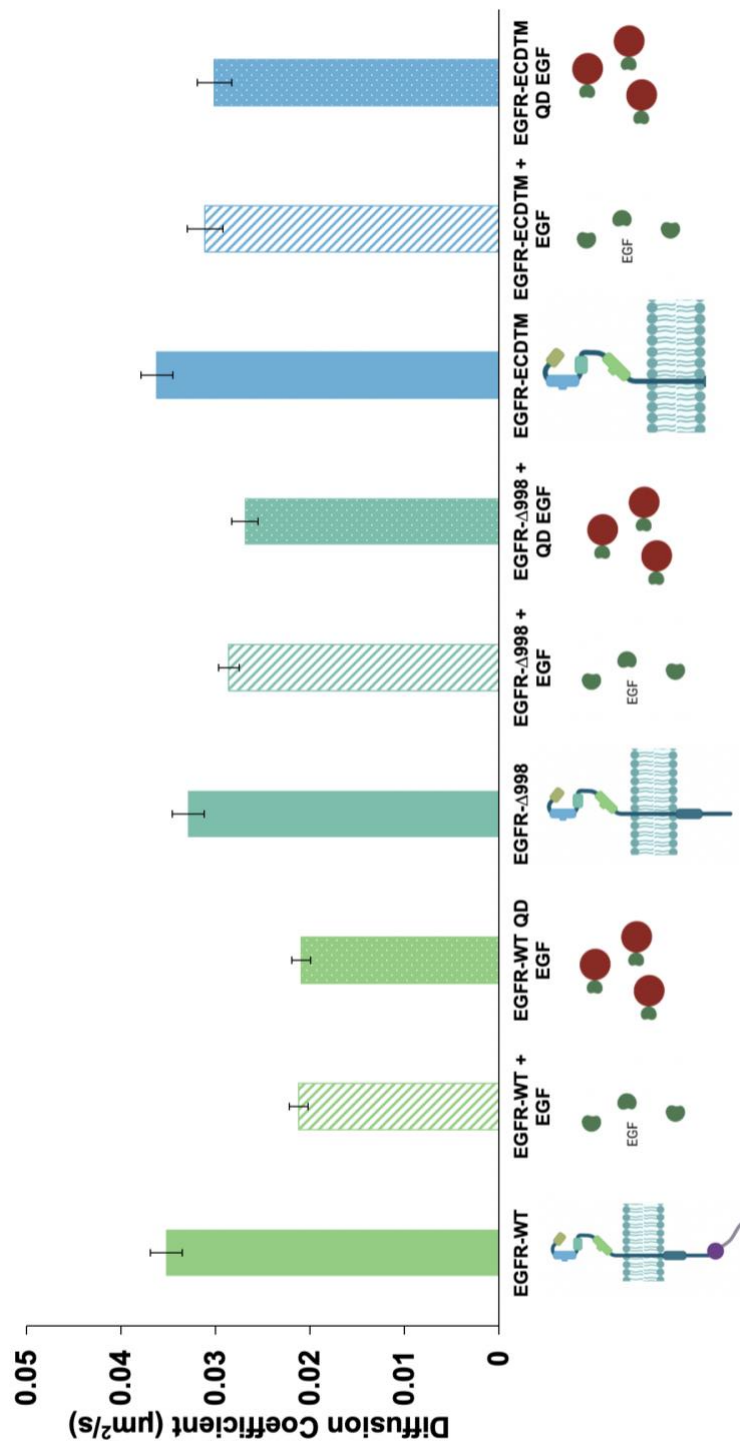
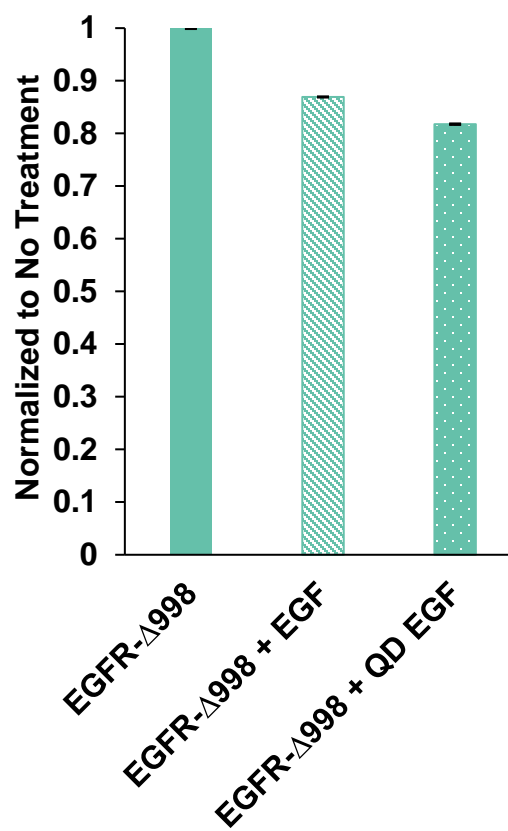
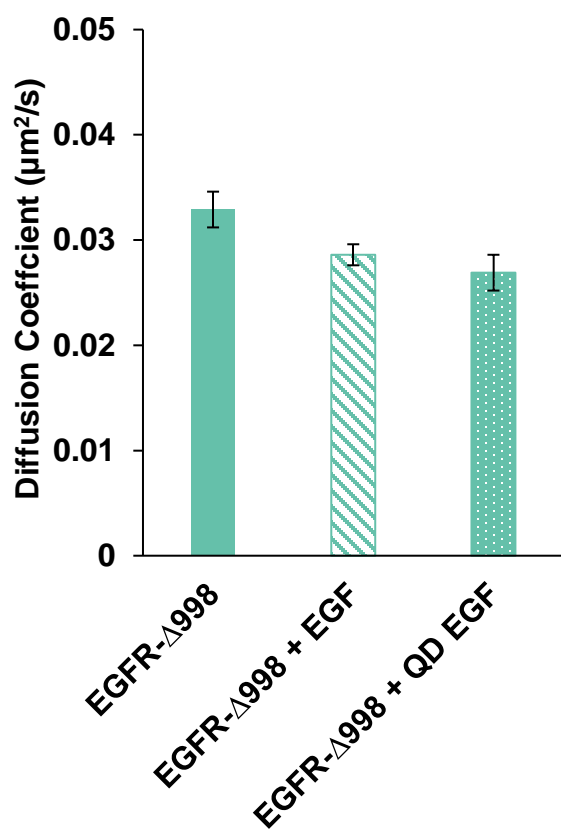
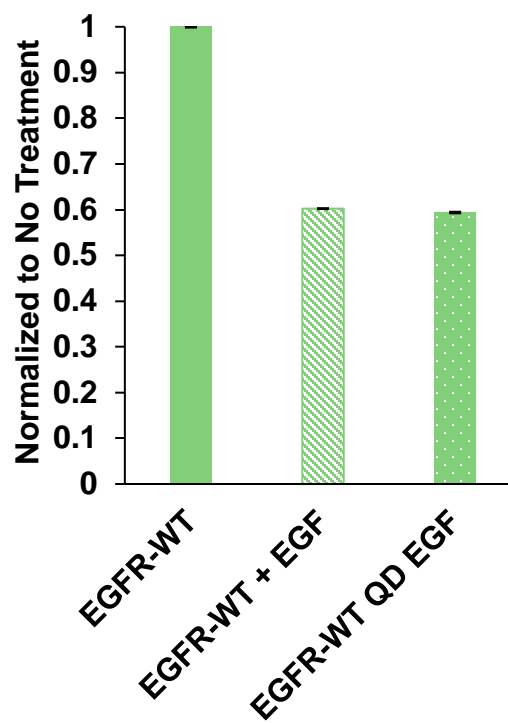
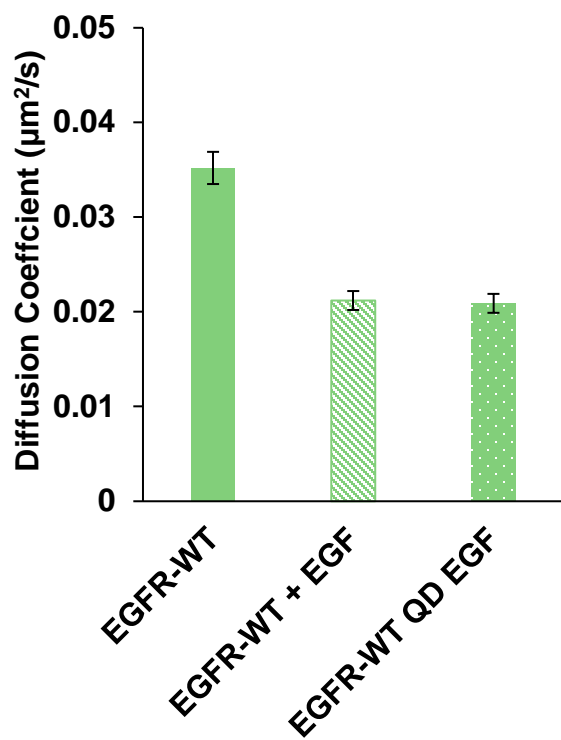


Figure 18. Diffusion coefficients for SPT of QD655- α -HA: HA-EGFR-WT, HA-EGFR- Δ 998 & HA-EGFR-ECDTM \pm Dark EGF or QD655-EGF. Bar graph displays a summary of diffusion coefficients for all conditions. EGFR-WT and EGFR- Δ 998 have a response to both methods of stimulation but, EGFR-ECDTM does not. Diffusion coefficients are from the fit of the ensemble MSD plots and error bars indicate 95% confidence interval. (Protein figures created with BioRender.com)



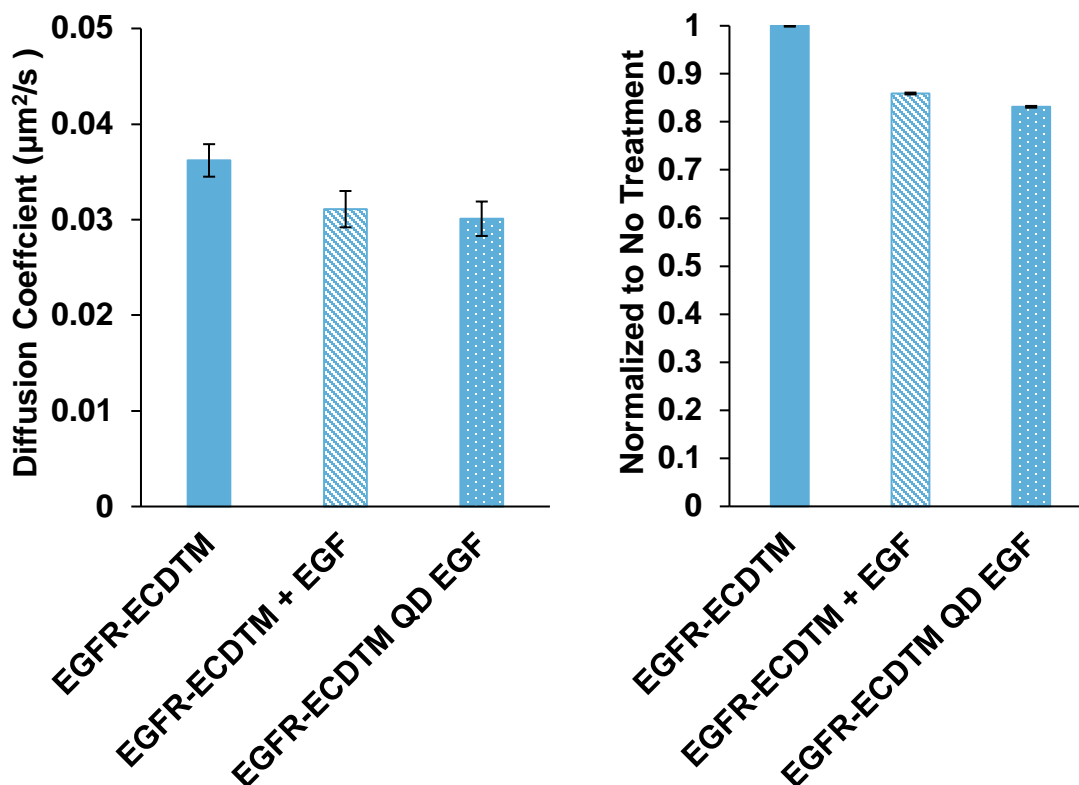


Figure 19. Diffusion coefficients QD655- α -HA: HA-EGFR-WT, HA-EGFR- Δ 998 & HA-EGFR-ECDTM \pm Dark EGF or QD655-EGF. Top Left: bar graph displays the diffusion coefficients for EGFR-WT no treatment, + 25 nM EGF and + 400 pM QD655-EGF. Top Right: Bar graph displays normalized values to the resting or, no treatment, state. Significant decrease in mobility is observed. Middle Left: bar graph displays the diffusion coefficients of EGFR- Δ 998 with no treatment, + 25 nM EGF and + 400 pM QD655-EGF. Middle Right: Bar graph displays normalized values to the resting or, no treatment, state. Significant decrease in mobility is observed. Bottom Left: bar graph displays the diffusion coefficient for EGFR-ECDTM no treatment, + 25 nM EGF and + 400 pM QD655-EGF. Bottom Right: Bar graph displays normalized values to the resting or, no treatment, state. No significant decrease in mobility is observed. Diffusion coefficients are from the fit of the ensemble MSD plots and error bars indicate 95% confidence interval.

EGFR HMM Preliminary Results

We took a deep dive into characterizing the mobility of the proteins and their decrease in diffusion but, the results obtained do not provide any information regarding the dimerization state of the truncation mutants. Characterizing the dimerization state of the truncation mutants can help reveal information on the extent to which dimerization contributes to signaling. The results obtained from using one-color QD tracking were used for the analysis and results of all previous sections however, two-color QD data was collected for each of the experiments. The data analysis of the two-color QD tracking is ongoing, but the discussion of preliminary results can be found below.

Two-color quantum dot tracking allows for the visualization of dimers that form between proteins; due to its ability to distinguish between two spectrally distinct QDs even when they are within the diffraction limit. Whether we are tracking one or two colors, the SPT experimental techniques described previously are applied in the same way. The experimental setup for SPT requires an extra component when tracking two colors. The emitted light must be split into two channels to capture the emitted light from two distinctly colored QDs (QD605 & QD655). The separation is necessary to distinguish between QDs upon analysis. As part of the experimental setup, filters were put in place to separate the emission into two distinct quadrants of the camera by using a Carin Optosplit two-channel splitter. Once cells were tracked under various conditions, a Hidden Markov Model (HMM) analysis produced k_{off} rates. Off rates (k_{off}) reflect receptor reaction kinetics, which allows us to differentiate between monomeric versus dimeric state behavior and that gives insight into the longevity of the dimeric states.

As previously described in sections 1.7 and 2.2.5, HMM analysis provided us with a further look into the dimerization of EGFR-FLWT and the truncation mutants. The calculated distances between the QDs combined with implemented thresholds allowed us to characterize the distances as either close enough to be considered dimers (state 2) or far enough to be considered free and independent (state 1), as shown in **Figure 20**.

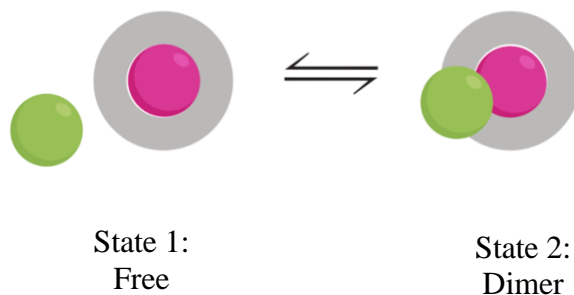


Figure 20. Depiction of HMM model states 1 and 2. Equilibrium between HMM model states one and two. The green sphere represents a QD of one-color (QD605) that appears in its respective channel while the pink sphere represents a QD of a different color (QD655) that appears in its respective channel. The gray area represents the separation threshold between the QDs that is used to distinguish between a dimer state and free state. (Created with BioRender.com)

This two-state hidden Markov model (HMM) required MATLAB®⁶⁰ to calculate the preliminary estimates of k_{off} for EGFR-WT and EGFR truncation mutants shown in **Figure 21**. These estimates reveal a higher k_{off} for non-liganded (no treatment) EGFR-WT when compared to the ligand-bound (+QD655-EGF) form. One could associate a higher k_{off} with shorter-lived (or transient) dimers, while a lower k_{off} (as seen for QD-EGF) indicates longer-lived or more stable dimers. These preliminary results are promising as they display the expected trends for the EGFR-WT. Upon EGF stimulation, EGF-bound dimers seem to be longer lived than unliganded dimers. The mutant data suggests that the EGFR- Δ 998 can also

form stable dimers upon EGF stimulation, as expected, while the EGFR-ECDTM appears to dimerize and maintain longer-lived (more stable) dimers even in the absence of EGF.

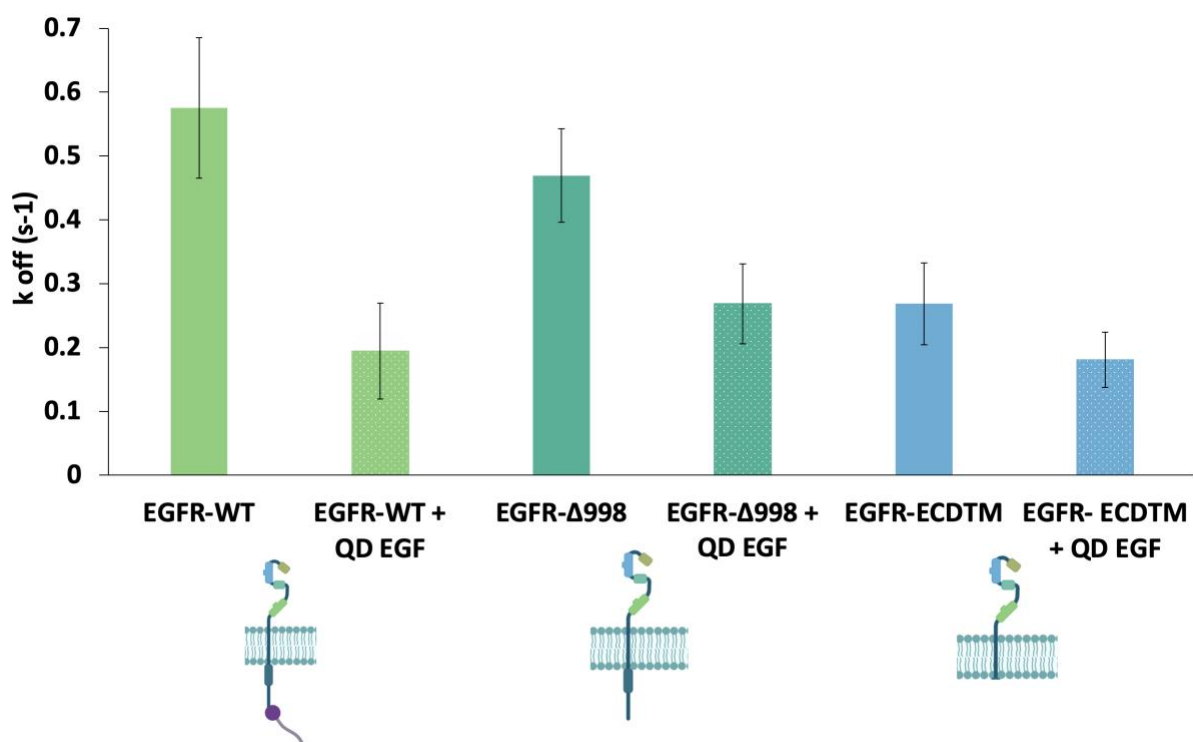


Figure 21. k_{off} rates of EGFR-WT, EGFR Δ 998, EGFR-ECDTM \pm 400 pM QD655-EGF & QD605-EGF preliminary estimates. EGFR k_{off} rates decreases upon QD605-EGF and QD655-EGF addition for both EGFR-WT and EGFR Δ 998. EGFR-ECDTM has a slower k_{off} even in the absence of ligand and this does not significantly change with EGF. (EGFR figures Created with BioRender.com)

The results are preliminary since a larger quantity of dimers is required to make conclusions. More two-color tracking data must be collected before making any dimerization conclusions regarding the receptor proteins in this two-color particle tracking study. We will also take a comprehensive approach to refine the codes used for the HMM analysis by producing results that enable visual inspection of the receptor's relative motion. For example, trajectories of two receptors moving with correlated motion over time could serve as a

confirmation checkpoint of the dimerization states of proteins. Additionally, jump correlation would help confirm if the receptors are found within proximity due to chance or if the receptors are making movements in unison as expected for bona fide dimers. Once the HMM analysis is refined, we hope to analyze the SPT data for each previous section in this study. By doing so, not only would we have insight into how the mobility of proteins correlates to signaling, but we would also conclude the dimerization states.

EGFR-RON crosstalk

In the previous sections, we have examined the connection between signaling and mobility for EGFR. As discussed in Chapter 1, RTKs can undergo hetero-interactions that may alter signaling outcomes. There are instances in which proteins participate in crosstalk, which provides them with alternative activation and signaling routes. These events can be linked to therapeutic resistance as targeted therapies often fail to target all proteins involved in mechanisms of activation due to a lack of evidence surrounding the specific roles that various proteins can play. Recent studies revealed that EGFR and RON participate in crosstalk.⁴⁴ In the following sections, we will use SPT to understand if the crosstalk between RON and EGFR takes place at the plasma membrane and what interactions are needed for RON activation or phosphorylation.

This portion of my study pertains to a larger project in the Lidke Lab that focuses on understanding EGFR-RON crosstalk, the results of which are currently under review.⁴⁴ A biochemical approach confirmed the observation in Franco Nitta *et. al*; that EGF-stimulated EGFR can phosphorylate RON, even in the absence of RON's ligand (MSP). A431 cells that express endogenous EGFR were transfected with HA-RON to generate a stable cell line. For Western Blot analysis, cells were left untreated or stimulated for 5 minutes with either 50 nM

EGF or 5 nM MSP. The cells were lysed for protein harvest, and western blots were run. The summary of the results is in **Figure 22**. The bands in the 700 nm channel (Green) in **Figure 22** indicate the presence of RON (top) and the presence of EGFR (bottom). The bands in the 800 nm channel (red) represent the phosphorylation state of the specific receptor. The third “channel” is an overlay of the two and will be used to draw conclusions. First, the control (or unstimulated condition) confirms the presence of the protein. No significant phosphorylation resulted for this condition. Second, we confirmed that with the addition of 5 nM MSP, RON becomes phosphorylated, as expected. Third and most importantly, the overlay of the channels reveals significant phosphorylation of HA-RON when cells were stimulated with 50 nM EGF. Recall that the phosphorylation occurred in the absence of RON’s ligand, MSP. This observation further reinforces the notion that RON does not require MSP for phosphorylation as it can result from EGF stimulation in the presence of EGFR.

Figure 17 shows that the reverse is not true. The presence of EGFR is confirmed in the control (or un-stimulated condition), 5 nM MSP, and 50 nM EGF conditions but, the overlay reveals that phosphorylation only occurs as a result of EGF stimulation and not due to MSP stimulation. This observation indicates that the mechanism that enables EGFR and RON to crosstalk is unidirectional, meaning that EGFR activation can result in RON phosphorylation but, RON activation does not result in EGFR phosphorylation, at least not with MSP stimulation.

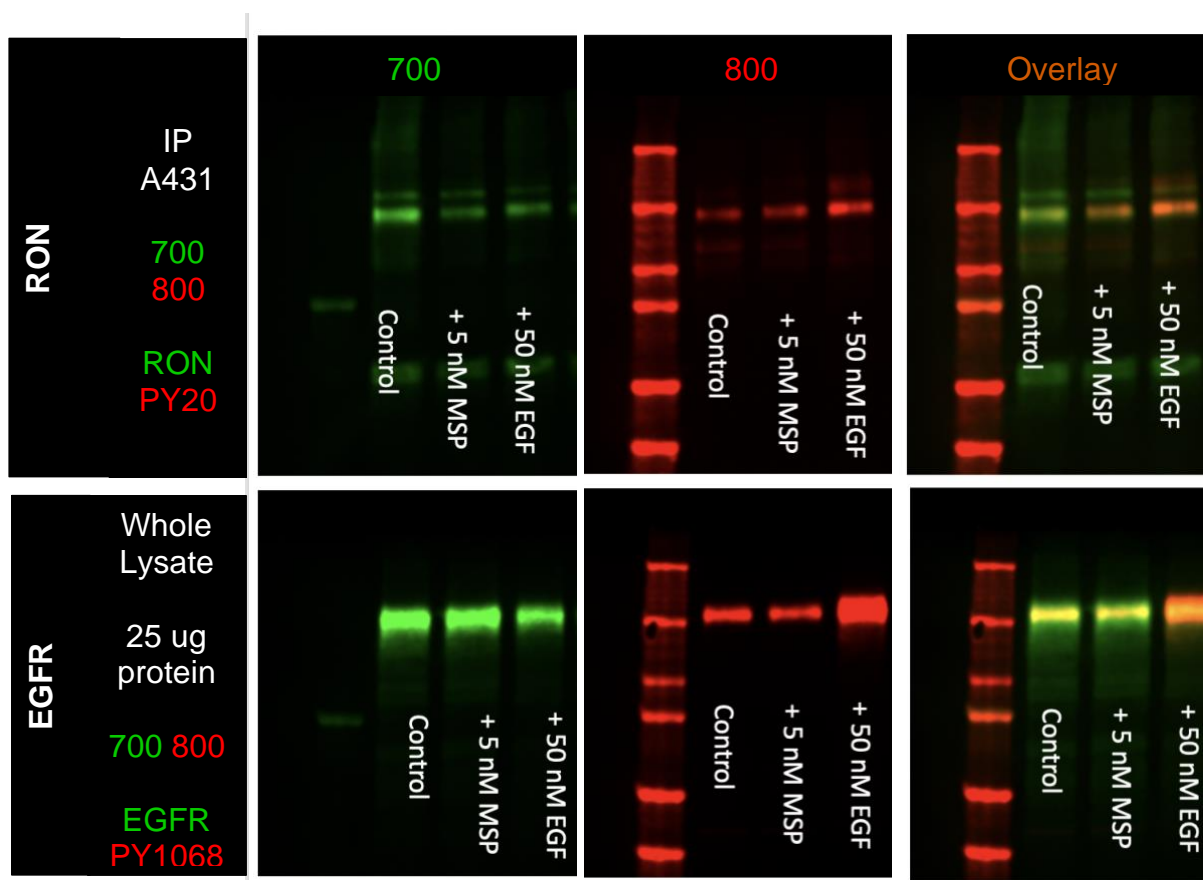


Figure 22. Immunoblot of A431 HA RON cells were treated with 5 nM MSP, 50 nM EGF or left untreated. Primary and secondary antibodies were used to blot for EGFR, RON and phosphorylation of the two proteins. RON required immunoprecipitation for further purification. Left: The green bands indicate the presence of the proteins, top is HA-RON and bottom is EGFR. Middle: Red bands indicate the phosphorylation state of the proteins. Middle top shows respective phosphorylation state of PY20 and PY99 sites pertaining to RON and bottom shows the phosphorylation state of EGFR's PY1068 phosphorylation site. Right: Overlay of the two previous channels where an orange band indicates phosphorylation. Top right shows confirmation of RON phosphorylation in the presence of 50 nM EGF.

SPT of QD655-HA-RON at the cell's surface (as shown in **Figure 23**) was performed using A431 cells co-expressing HA-RON and endogenous EGFR to further explore the crosstalk dynamics occurring between RON and EGFR.

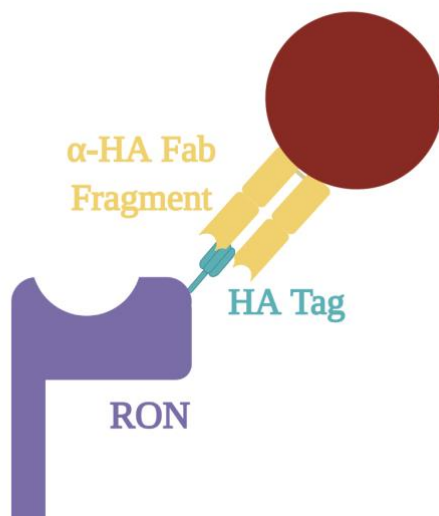
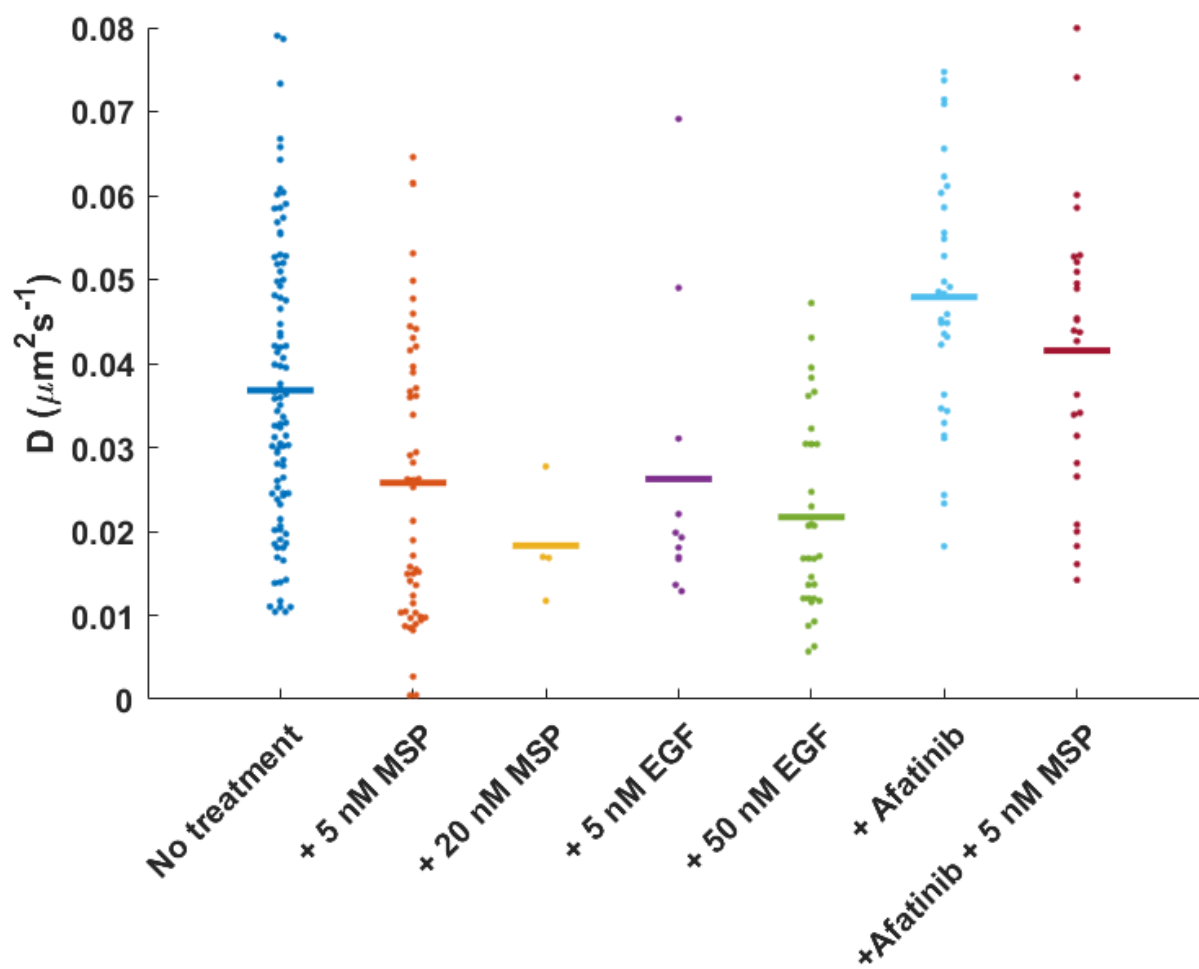


Figure 23. HA-RON & HA-RON K1114M QD labeling A Biotinylated α -HA fab fragment that binds to a streptavidin coated QD was used to label the H-tag on the extracellular domain of RON. (Created with BioRender.com)

A variety of conditions were implemented, starting with MSP stimulation for control purposes. **Figures 24, 25, and 26** show the diffusion results of tracking HA-RON with no ligand, 5 nM MSP, and 20 nM MSP. Based on our SPT results of EGFR, we would expect RON to slowdown when stimulated by ligand. As expected, MSP causes RON's diffusion to decrease in a dose-dependent manner, such that the higher concentration of MSP results in a greater mobility decrease. 5 nM MSP results in a diffusion decrease of $0.0101 \pm 0.0031 \mu\text{m}^2/\text{s}$ ($\approx 27\%$) while 50 nM results in a $0.0188 \pm 0.0022 \mu\text{m}^2/\text{s}$ ($\approx 50\%$) decrease. The greater decrease in diffusion can be a result of ligand accessibility, a higher concentration of ligand can result in a higher concentration of ligand-bound proteins. This, in turn, results in enhanced protein dimerization, phosphorylation, and downstream signaling. Interestingly the dynamic results reveal a similar trend is observed for varying EGF concentrations where a higher concentration of EGF results in a greater diffusion slowdown for HA-RON. The 5 nM EGF treatment resulted in a diffusion decrease of $0.0118 \pm 0.0039 \mu\text{m}^2/\text{s}$ ($\approx 32\%$) while the 50 nM EGF elicited a

diffusion decrease of $0.0152 \pm 0.0035 \mu\text{m}^2/\text{s}$ ($\approx 41\%$). Moreover, the slowdown resulting from EGF stimulation serves as further validation of EGFR-RON crosstalk. Based on our interpretation of a decrease in mobility, the results allow us to conclude that RON dimerization, phosphorylation, protein recruitment, or a combination of these events occurs due to MSP and EGF stimulation. These dynamic results further support the biochemical results obtained by Dr. Franco Nitta. RON is phosphorylated upon EGF stimulation when co-expressed with endogenous EGFR. **Table 3** provides a summary of the values including errors and significance.



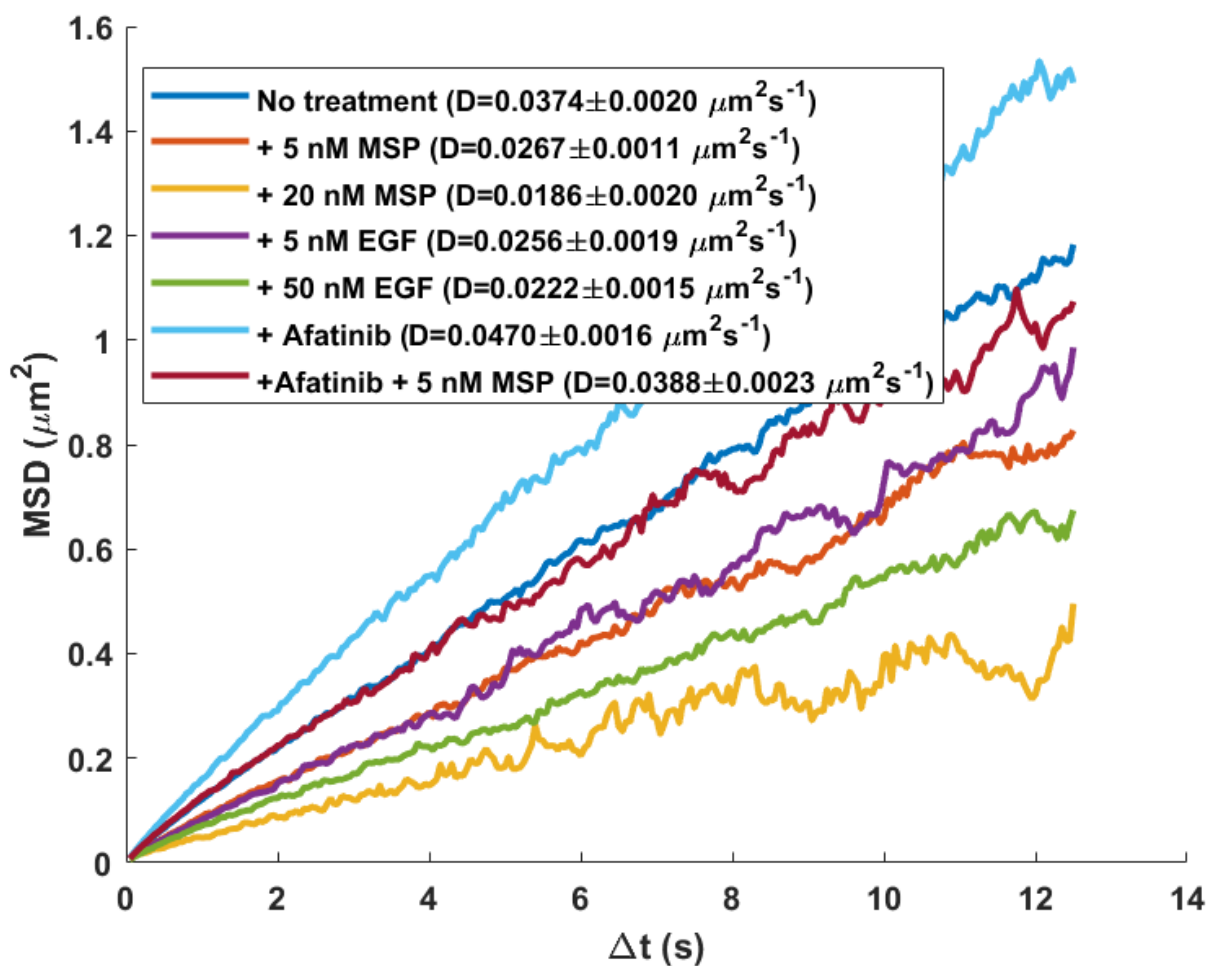


Figure 24. Plots comparing RON mobility without treatment, + 5 nM MSP, + 20 nM MSP, + 5 nM EGF, + 50 nM EGF, + 10 μm Afatinib and + 10 μm Afatinib and 5 nM EGF. SPT results overview Top: Beeswarm Plot displays each cell's diffusion coefficient result in the form of a dot and the averaged value as a horizontal bar. Bottom MSD plot displays ensemble mean squared displacement where a decrease in slope is indicative of slower mobility. Results were plotted for 96 untreated cells, 53- 5 nM MSP treated cells, 5- 20 nM MSP treated cells, 12- 5 nM EGF treated cells, 32- 50 nM EGF treated cells, 33- 10 μm Afatinib treated cells and 27-10 μm Afatinib and 5 nM MSP.

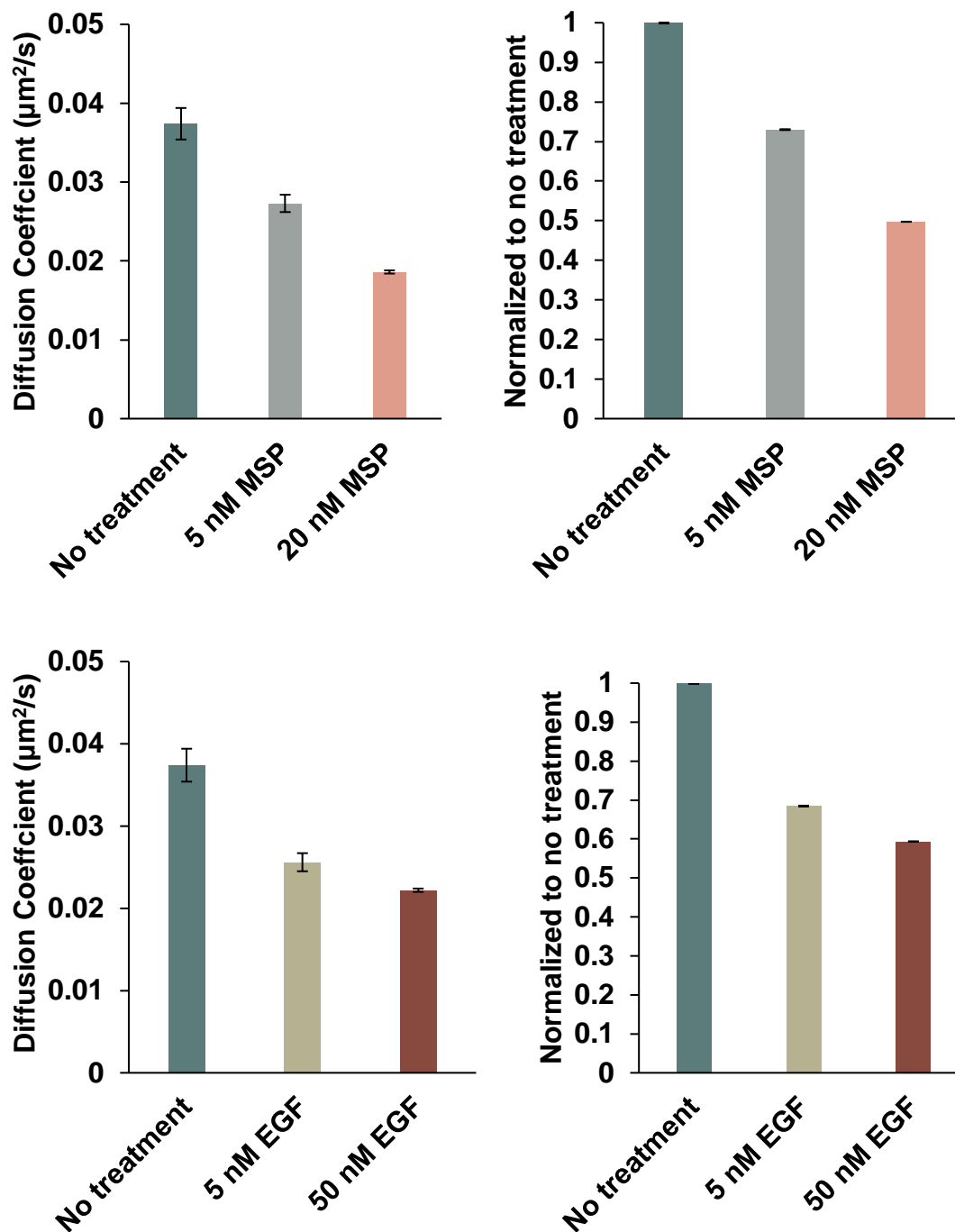


Figure 25. Diffusion coefficients for SPT of QD655-HA-RON in A431 HA-RON. Top Left: bar graph displays the diffusion coefficient for HA-RON no treatment, + 5 nM MSP and + 20 nM MSP. Top Right: Bar graph displays normalized values to the resting or, no treatment, state. There is a dose-dependent response to MSP. Bottom Left: bar graph displays the diffusion coefficients for HA-RON under no treatment, + 5 nM EGF and + 50 nM QD655-EGF. Bottom Right: Bar graph displays normalized values to the resting or, no treatment, state.

There is also a dose-dependent response to EGF. Diffusion coefficients are from the fit of the ensemble MSD plots and error bars indicate 95% confidence interval.

The data revealed that EGFR plus EGF stimulation results in RON activation. Therefore, we wanted to explore the potential effects of EGFR inhibition on RON's response to its ligand (MSP). For this study, we introduced a well-known EGFR inhibitor, Afatinib (at 10 μm) which would prevent EGFR's kinase activation (as shown in section 3.3) and performed the same SPT techniques. Cells were treated with 10 μm of Afatinib for 15 minutes prior to SPT of HA-RON. **Figures 24 and 26** show the results of the diffusion measurements obtained from those experiments. The inhibition of EGFR does influence RON's mobility. In their resting (unstimulated) forms, the cells treated with 10 μm Afatinib resulted in mobility about $\approx 26\%$ higher than the non-inhibited form. This difference was deemed significant by a two-tail t-test of unequal variances ($p < 0.05$) hinting that Afatinib can influence RON's mobility. One can deduce that the mobility decrease for the cells treated with Afatinib is less significant than the one observed for the non-treated cells upon MSP stimulation. The non-treated cells resulted in about a $\approx 27\%$ diffusion decrease, while the cells that were treated with 10 μm Afatinib had a $\approx 17\%$ diffusion decrease. Although the responses seem different, they indicate that the Afatinib treatment did not prevent RON's slowdown when stimulated.

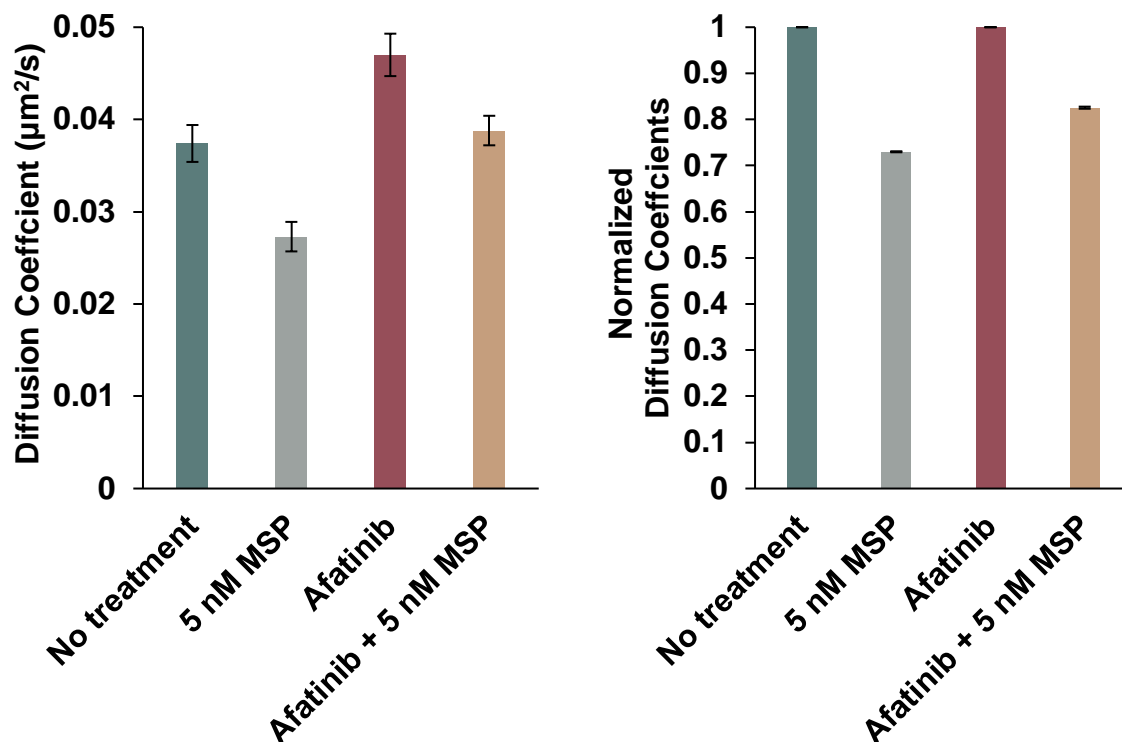


Figure 26. Diffusion coefficients for SPT of HA-RON \pm 5 nM MSP, \pm 10 μm Afatinib, \pm 10 μm Afatinib and 5 nM MSP. Left: bar graph displays the diffusion coefficients of HA RON no treatment, + 5 nM MSP, + 10 μm Afatinib, and + 10 μm Afatinib in combination with + 5 nM MSP. Right: Bar graph displays normalized diffusion coefficients for 5 nM MSP result to the resting or, no treatment, state while the 10 μm Afatinib + 5 nM MSP diffusion coefficient is normalized to + 10 μm Afatinib state. Diffusion coefficients are from the fit of the ensemble MSD plots and werror bars indicate 95% confidence interval.

Table 3. Results summary for A431 HA RON, $\pm 10 \mu\text{m}$ Afatinib, ± 5 or 20 nM MSP, or ± 5 or 50 nM EGF including errors and statistical analysis. The difference in RON's mobility between its resting, or non-treated form conditions + 5 nM MSP, + 20 nM MSP, + 5 nM EGF, 50 nM EGF and $10 \mu\text{m}$ Afatinib were all statistically significant. Mobility was significantly decreased when RON was treated with $10 \mu\text{m}$ Afatinib and stimulated with 5 nM MSP.

Variable 1	Average diffusion ($\mu\text{m}^2/\text{s}$)	Error (\pm)	Variable 2	Averaged Diffusion ($\mu\text{m}^2/\text{s}$)	Error (\pm)	Difference ($\mu\text{m}^2/\text{s}$)	Error (\pm)	% Decrease	P value (2-tail)	Significant
A431 HA RON	0.0374	0.002	A431 HA RON + 5 nM MSP	0.0273	0.0011	0.0101	0.0031	27%	0.000264	✓
A431 HA RON	0.0374	0.002	A431 HA RON + 20 nM MSP	0.0186	0.0002	0.0188	0.0022	50%	0.004494	✓
A431 HA RON	0.0374	0.002	A431 HA RON + 5 nM EGF	0.0256	0.0019	0.0118	0.0039	32%	0.040661	✓
A431 HA RON	0.0374	0.002	A431 HA RON + 50 nM EGF	0.0222	0.0015	0.0152	0.0035	41%	3.61E-07	✓
A431 HA RON	0.0374	0.002	A431 HA RON + Afatinib	0.047	0.0016	-0.0096	0.0036	-26%	0.000819	✓
A431 HA RON + Afatinib	0.047	0.0016	A431 HA RON + Afatinib + 5 nM MSP	0.0388	0.0023	0.0082	0.0039	17%	0.021914	✓

As previously shown, the mobility of a receptor can indicate a receptor's dimerization, phosphorylation, and or protein recruitment state. Like the EGFR truncation mutant experiment, a kinase-dead mutant of RON (K1114M) was studied in combination with its wild-type form to compare the impact that EGF stimulation had on the overall mobility of the proteins. The kinase-dead mutant prevented RON's kinase from autophosphorylating itself. Phosphorylation events resulting from this mutated version of RON would have to be due to external factors such as crosstalk. **Figure 28** shows a bar graph depicting the diffusion results for the WT and RON-K1114M. We can appreciate an almost identical response to EGF by RON-K1114M, the kinase-dead version of RON when compared to its WT counterpart. RON WT's diffusion decreased by $0.0122 \pm 0.0012 \mu\text{m}^2/\text{s}$ while the mutated form decreased by $0.0117 \pm 0.0014 \mu\text{m}^2/\text{s}$. The results coincide with a $\approx 38\%$ decrease in mobility, indicating that EGFR can directly phosphorylate RON upon stimulation with EGF (as shown in **Figure 27**) and that RON's kinase domain is not required for crosstalk propagation.

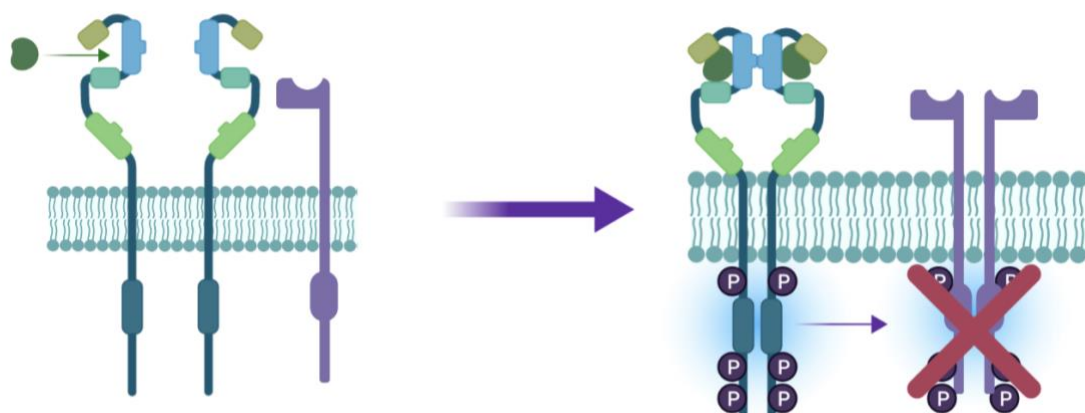


Figure 27. EGFR stimulation results in RON Phosphorylation and does not require RON's kinase activity. When co-expressed, EGFR is able to directly phosphorylate RON's kinase to propagate crosstalk through an unknown mechanism. (Created with BioRender.com)

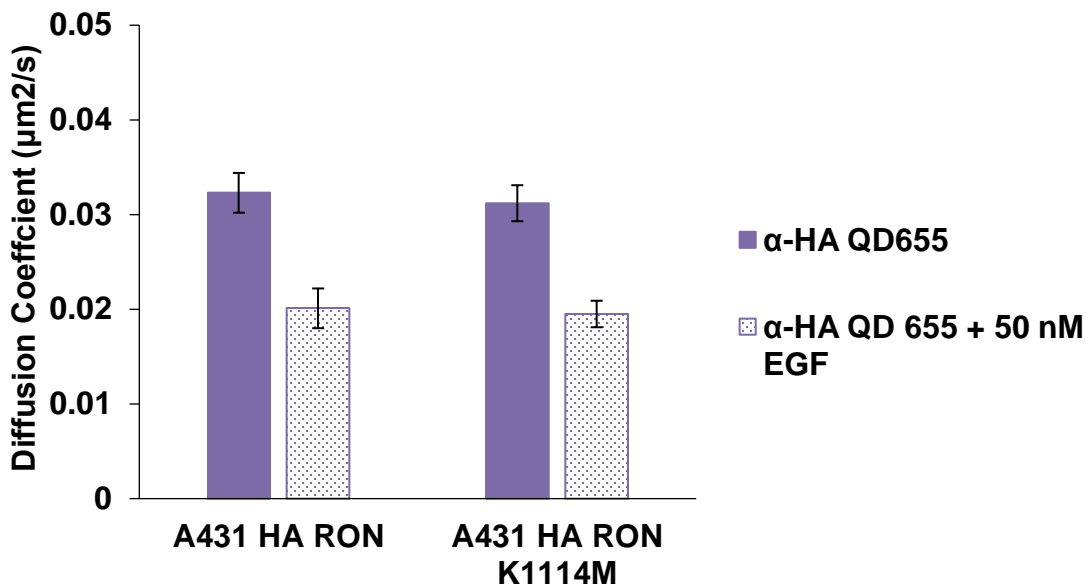


Figure 28. Diffusion coefficients for SPT of A431 HA-RON and A431 HA RON K1114 α -HA-QD655 \pm 50 nM EGF. Bar graph displays the diffusion coefficients for HA-RON and A431 HA RON K1114 (kinase dead form) with no treatment and + 50 nM EGF. Both cases show a significant response to 50 nM EGF stimulation. RON's kinase activity is not required for EGF-driven slowdown or phosphorylation of RON. Diffusion coefficients are from the ensemble MSD plots and error bars indicate 95% confidence interval.

The results derived from this study further support evidence of RON phosphorylation upon EGF stimulation when the receptor is co-expressed with EGFR, regardless of its kinase functionality.^{3,61} In a pathological context, the observation can indicate the presence of a therapeutic escape route, suggesting an alternative mechanism for RON phosphorylation/activation that leads to downstream signaling. Considering that RON-EGFR co-expression has led to a worse prognosis for patients and that monotherapies targeting RON have failed to succeed,^{3,62} one can infer that therapies that target RON without addressing EGFR (or the crosstalk occurring between the receptors) are risking therapeutic failure due to RON's alternative activation route, which would continue to drive oncogenesis.

CHAPTER 4

SUMMARY

The conclusions produced by this study confirm that EGFR stimulation with EGF results in a significant mobility decrease. The observation further supports the trends observed by previous studies in which unliganded EGFR-WT (resting) had higher mobility when compared to its ligand-bound counterpart.^{12,32} Previous studies postulated that the observed slowdown was due to the recruitment of accessory proteins to the activated receptor complex, and this study looked directly into that possibility. Although we did not detect the contribution that the two adaptor proteins, Shc1 and Grb2, had on the receptor's mobility, we determined that the absence of the C-terminal tail of EGFR (EGFR- Δ 998 mutation) did not elicit the same response as it did for EGFR-WT. The modest decrease in mobility of EGFR- Δ 998 upon EGF stimulation might be a result of dimerization and serves as further confirmation that the recruitment of accessory proteins must be present to observe the full slowdown. Based on these results, we can predict that the diffusion decrease observed for EGFR- Δ 998 was a result of a non-signaling dimer formation. Conversely, the full slowdown only results from the recruitment of accessory proteins to the activated receptor complex. Therefore, although our measurements can reflect dimerization, receptor signaling is the principal readout of receptor mobility.

The diffusion decrease upon EGF stimulation of EGFR-ECDTM (missing the entire intracellular region) was not significant compared to the diffusion decrease of EGFR-WT (upon EGF stimulation). There are a few possible explanations for this. The absence of even a modest slowdown can indicate that EGFR-ECDTM might not be capable of forming dimers, or perhaps part of the kinase domain (besides the C-terminal tail) must be present to induce a

significant decrease in mobility. Another reason could lie behind the experimental and analytical methods used for this study. There is a possibility that the slowdown upon EGF stimulation might be too small to detect in EGFR-ECDTM. If we take the HMM results into account, we could predict that the truncation mutant was in a dimer conformation prior to EGF addition. If this were true, then we would fail to see any slowdown. Further studies of other EGFR truncation mutants may help reveal which specific parts of the kinase domain elicit decreases in mobility and which are required for dimer formation and dimer stability.

When studying the effect of ligand concentration on RON's mobility, we determined there is a dose-dependent response to both MSP and EGF (EGFR's ligand), further supporting the observations of other studies.⁴⁴ The studies focused on the crosstalk dynamics between EGFR and RON revealed that EGFR can activate RON unidirectionally. The rapid slowdown observed for RON upon EGF stimulation indicates that these interactions occur the plasma membrane. When we looked at HA-RON-K1114M (kinase-dead mutant) we confirmed this to be true. RON's kinase activity is not needed to observe a slowdown in mobility, indicative of activation/phosphorylation, and we predict that EGFR's kinase is responsible for this.

Furthermore, we were able to confirm that adding an EGFR inhibitor, Afatinib, does have a significant impact on RON's overall motility in its resting state, hinting that EGFR does play a role in RON's mobility. In addition, when we added RON's ligand (MSP) to the Afatinib-treated cells, we still observed a significant response as a decrease in RON mobility. This observation reveals that EGFR inhibition does not impact RON's ability to phosphorylate when stimulated with its own ligand, which supports the biochemical results from our previous study by Franco Nitta *et.al*⁴⁴. Furthermore, that same study revealed⁴⁴ that EGFR inhibition with PD153035 (reversible kinase inhibitor) does block EGF-induced RON slowdown and that

Afatinib (non-reversible inhibitor) completely blocked EGF-dependent RON phosphorylation but, the results have yet to be confirmed biophysically.

The findings of this study helped characterize the readout that we obtain from dynamic studies of protein receptors. It revealed that slowdown in protein mobility is a result of, and a readout for signaling. The findings also allowed us to better understand the structure-function relationship of EGFR, one of the most important receptors involved in oncogenic signaling pathways. The implications of the results surrounding the crosstalk between RON and EGFR can help explain why cancer monotherapies often fail. We have provided evidence of a potential source of therapeutic resistance that involves RON's activation by EGFR even when RON's kinase activity is blocked. Moreover, this observation serves to support the use of multitarget therapy applications.

CHAPTER 5

FUTURE DIRECTIONS

The contents of this study revealed interesting details surrounding protein dynamics in the oncogenic signaling context. Undoubtedly, other studies are necessary to continue enhancing our understanding of RTK structure-function relationships. Regarding EGFR, there is one truncation mutant we intended to investigate as part of this study but could not due to difficulties we faced with the generation of a stable cell line expressing this mutant. The truncation mutant, EGFR-TMKD, lacked the entire extracellular region and was composed of the transmembrane (TM) and kinase domain (KD) only. We hoped to investigate the truncation mutant's phosphorylation through dynamic measurements obtained using the same SPT techniques previously described here. We wanted to determine if the EGFR-TMKD mutant was capable of phosphorylation. The mutant lacked structural components required for ligand binding and dimerization but, we do not know if phosphorylation is possible. The generation of stable cell lines containing this mutant or other truncation mutants could further reveal important details surrounding EGFR's structure-function relationship.

We know that EGFR point mutations and deletions occurring in exons 18–25 are associated with decreased patient response to treatments.⁶³ Analyzing specific mutants through a molecular dynamic lens could also help advance our understanding of their signaling capabilities. These types of studies can potentially reveal information surrounding targeting opportunities for treatment development. Following the steps outlined in this study would be a perfect starting point to study a variety of mutants, each of them revealing a piece of a much greater picture.

REFERENCES

- (1) The Cooperative Human. *Nature Human Behaviour* **2018**, 2 (7), 427–428. <https://doi.org/10.1038/s41562-018-0389-1>.
- (2) The discovery of receptor tyrosine kinases: targets for cancer therapy | Nature Reviews Cancer <https://www.nature.com/articles/nrc1360> (accessed 2021 -02 -01).
- (3) Keller, J.; Nimmual, A. S.; Shroyer, K. R.; Joy, C.; Ischenko, I.; Chandler, C. S.; Dong, L. M.; Hayman, M. J.; Chan, E. L. Ron Tyrosine Kinase Receptor Synergises with EGFR to Confer Adverse Features in Head and Neck Squamous Cell Carcinoma. *British Journal of Cancer* **2013**, 109 (2), 482–492. <https://doi.org/10.1038/bjc.2013.321>.
- (4) And, R. L.-M.; Cohen, S. Effects of the Extract of the Mouse Submaxillary Salivary Glands on the Sympathetic System of Mammals*. *Annals of the New York Academy of Sciences* **1960**, 85 (1), 324–341. <https://doi.org/10.1111/j.1749-6632.1960.tb49963.x>.
- (5) Cochet, C.; Gill, G. N.; Meisenhelder, J.; Cooper, J. A.; Hunter, T. C-Kinase Phosphorylates the Epidermal Growth Factor Receptor and Reduces Its Epidermal Growth Factor-Stimulated Tyrosine Protein Kinase Activity. *J. Biol. Chem.* **1984**, 259 (4), 2553–2558.
- (6) Garrett, T. P. J.; McKern, N. M.; Lou, M.; Elleman, T. C.; Adams, T. E.; Lovrecz, G. O.; Zhu, H.-J.; Walker, F.; Frenkel, M. J.; Hoyne, P. A.; Jorissen, R. N.; Nice, E. C.; Burgess, A. W.; Ward, C. W. Crystal Structure of a Truncated Epidermal Growth Factor Receptor Extracellular Domain Bound to Transforming Growth Factor β . 11.
- (7) He, L.; Hristova, K. Physical–Chemical Principles Underlying RTK Activation, and Their Implications for Human Disease. *Biochimica et Biophysica Acta (BBA) - Biomembranes* **2012**, 1818 (4), 995–1005. <https://doi.org/10.1016/j.bbamem.2011.07.044>.
- (8) Sigismund, S.; Avanzato, D.; Lanzetti, L. Emerging Functions of the EGFR in Cancer. *Mol Oncol* **2018**, 12 (1), 3–20. <https://doi.org/10.1002/1878-0261.12155>.
- (9) The Membrane Mimetic Affects the Spatial Structure and Mobility of EGFR Transmembrane and Juxtamembrane Domains | Biochemistry <https://pubs-acsc-org.libproxy.unm.edu/doi/10.1021/acs.biochem.5b00851> (accessed 2021 -02 -10).

- (10) Lemmon, M. A.; Bu, Z.; Ladbury, J. E.; Zhou, M.; Pinchasi, D.; Lax, I.; Engelman, D. M.; Schlessinger, J. Two EGF Molecules Contribute Additively to Stabilization of the EGFR Dimer. *EMBO J* **1997**, *16* (2), 281–294.
<https://doi.org/10.1093/emboj/16.2.281>.
- (11) Burgess, A. W. EGFR Family: Structure Physiology Signalling and Therapeutic Targets †. *Growth Factors* **2008**, *26* (5), 263–274.
<https://doi.org/10.1080/08977190802312844>.
- (12) Valley, C. C.; Arndt-Jovin, D. J.; Karedla, N.; Steinkamp, M. P.; Chizhik, A. I.; Hlavacek, W. S.; Wilson, B. S.; Lidke, K. A.; Lidke, D. S. Enhanced Dimerization Drives Ligand-Independent Activity of Mutant Epidermal Growth Factor Receptor in Lung Cancer. *Mol. Biol. Cell* **2015**, *26* (22), 4087–4099.
<https://doi.org/10.1091/mbc.E15-05-0269>.
- (13) Lemmon, M. A.; Schlessinger, J.; Ferguson, K. M. The EGFR Family: Not So Prototypical Receptor Tyrosine Kinases. *Cold Spring Harb Perspect Biol* **2014**, *6* (4).
<https://doi.org/10.1101/cshperspect.a020768>.
- (14) Jones, S.; Rappoport, J. Z. Interdependent Epidermal Growth Factor Receptor Signalling and Trafficking. *The International Journal of Biochemistry & Cell Biology* **2014**, *51*, 23–28. <https://doi.org/10.1016/j.biocel.2014.03.014>.
- (15) Schlessinger, J. Ligand-Induced, Receptor-Mediated Dimerization and Activation of EGF Receptor. *Cell* **2002**, *110* (6), 669–672. [https://doi.org/10.1016/S0092-8674\(02\)00966-2](https://doi.org/10.1016/S0092-8674(02)00966-2).
- (16) Wee, P.; Wang, Z. Epidermal Growth Factor Receptor Cell Proliferation Signaling Pathways. *Cancers (Basel)* **2017**, *9* (5). <https://doi.org/10.3390/cancers9050052>.
- (17) Lewis, T. S.; Shapiro, P. S.; Ahn, N. G. Signal Transduction through MAP Kinase Cascades. *Adv Cancer Res* **1998**, *74*, 49–139. [https://doi.org/10.1016/s0065-230x\(08\)60765-4](https://doi.org/10.1016/s0065-230x(08)60765-4).
- (18) Lowenstein, E. J.; Daly, R. J.; Batzer, A. G.; Li, W.; Margolis, B.; Lammers, R.; Ullrich, A.; Skolnik, E. Y.; Bar-Sagi, D.; Schlessinger, J. The SH2 and SH3 Domain-Containing Protein GRB2 Links Receptor Tyrosine Kinases to Ras Signaling. *Cell* **1992**, *70* (3), 431–442. [https://doi.org/10.1016/0092-8674\(92\)90167-b](https://doi.org/10.1016/0092-8674(92)90167-b).

- (19) Jiang, X.; Huang, F.; Marusyk, A.; Sorkin, A. Grb2 Regulates Internalization of EGF Receptors through Clathrin-Coated Pits. *Mol Biol Cell* **2003**, *14* (3), 858–870. <https://doi.org/10.1091/mbc.e02-08-0532>.
- (20) Batzer, A. G.; Rotin, D.; Ureña, J. M.; Skolnik, E. Y.; Schlessinger, J. Hierarchy of Binding Sites for Grb2 and Shc on the Epidermal Growth Factor Receptor. *Mol Cell Biol* **1994**, *14* (8), 5192–5201. <https://doi.org/10.1128/mcb.14.8.5192-5201.1994>.
- (21) Pelicci, G.; Lanfrancone, L.; Grignani, F.; McGlade, J.; Cavallo, F.; Forni, G.; Nicoletti, I.; Grignani, F.; Pawson, T.; Pelicci, P. G. A Novel Transforming Protein (SHC) with an SH2 Domain Is Implicated in Mitogenic Signal Transduction. *Cell* **1992**, *70* (1), 93–104. [https://doi.org/10.1016/0092-8674\(92\)90536-1](https://doi.org/10.1016/0092-8674(92)90536-1).
- (22) Chardin, P.; Camonis, J. H.; Gale, N. W.; van Aelst, L.; Schlessinger, J.; Wigler, M. H.; Bar-Sagi, D. Human Sos1: A Guanine Nucleotide Exchange Factor for Ras That Binds to GRB2. *Science* **1993**, *260* (5112), 1338–1343. <https://doi.org/10.1126/science.8493579>.
- (23) Li, N.; Batzer, A.; Daly, R.; Yajnik, V.; Skolnik, E.; Chardin, P.; Bar-Sagi, D.; Margolis, B.; Schlessinger, J. Guanine-Nucleotide-Releasing Factor HSos1 Binds to Grb2 and Links Receptor Tyrosine Kinases to Ras Signalling. *Nature* **1993**, *363* (6424), 85–88. <https://doi.org/10.1038/363085a0>.
- (24) Boriack-Sjodin, P. A.; Margarit, S. M.; Bar-Sagi, D.; Kuriyan, J. The Structural Basis of the Activation of Ras by Sos. *Nature* **1998**, *394* (6691), 337–343. <https://doi.org/10.1038/28548>.
- (25) Brtva, T. R.; Drugan, J. K.; Ghosh, S.; Terrell, R. S.; Campbell-Burk, S.; Bell, R. M.; Der, C. J. Two Distinct Raf Domains Mediate Interaction with Ras. *J Biol Chem* **1995**, *270* (17), 9809–9812. <https://doi.org/10.1074/jbc.270.17.9809>.
- (26) Bondzi, C.; Grant, S.; Krystal, G. W. A Novel Assay for the Measurement of Raf-1 Kinase Activity. *Oncogene* **2000**, *19* (43), 5030–5033. <https://doi.org/10.1038/sj.onc.1203862>.
- (27) Genomic and biochemical insights into the specificity of ETS transcription factors - PubMed <https://pubmed-ncbi-nlm-nih-gov.libproxy.unm.edu/21548782/> (accessed 2021 -05 -28).

- (28) de Vos, A. M.; Ultsch, M.; Kossiakoff, A. A. Human Growth Hormone and Extracellular Domain of Its Receptor: Crystal Structure of the Complex. *Science* **1992**, 255 (5042), 306–312. <https://doi.org/10.1126/science.1549776>.
- (29) Ferguson, K. M.; Berger, M. B.; Mendrola, J. M.; Cho, H.-S.; Leahy, D. J.; Lemmon, M. A. EGF Activates Its Receptor by Removing Interactions That Autoinhibit Ectodomain Dimerization. *Molecular Cell* **2003**, 11 (2), 507–517. [https://doi.org/10.1016/S1097-2765\(03\)00047-9](https://doi.org/10.1016/S1097-2765(03)00047-9).
- (30) Two EGF molecules contribute additively to stabilization of the EGFR dimer | The EMBO Journal <https://www.embopress.org.libproxy.unm.edu/doi/full/10.1093/emboj/16.2.281> (accessed 2020 -10 -29).
- (31) Chung, I.; Akita, R.; Vandlen, R.; Toomre, D.; Schlessinger, J.; Mellman, I. Spatial Control of EGF Receptor Activation by Reversible Dimerization on Living Cells. *Nature* **2010**, 464 (7289), 783–787. <https://doi.org/10.1038/nature08827>.
- (32) Valley, C. C.; Lidke, K. A.; Lidke, D. S. The Spatiotemporal Organization of ErbB Receptors: Insights from Microscopy. *Cold Spring Harb Perspect Biol* **2014**, 6 (2). <https://doi.org/10.1101/cshperspect.a020735>.
- (33) Low-Nam, S. T.; Lidke, K. A.; Cutler, P. J.; Roovers, R. C.; van Bergen en Henegouwen, P. M. P.; Wilson, B. S.; Lidke, D. S. ErbB1 Dimerization Is Promoted by Domain Co-Confinement and Stabilized by Ligand-Binding. *Nat Struct Mol Biol* **2011**, 18 (11), 1244–1249. <https://doi.org/10.1038/nsmb.2135>.
- (34) Xiao, Z.; Ma, X.; Jiang, Y.; Zhao, Z.; Lai, B.; Liao, J.; Yue, J.; Fang, X. Single-Molecule Study of Lateral Mobility of Epidermal Growth Factor Receptor 2/HER2 on Activation. *J. Phys. Chem. B* **2008**, 112 (13), 4140–4145. <https://doi.org/10.1021/jp710302j>.
- (35) Di Guglielmo, G. m.; Baass, P. c.; Ou, W. j.; Posner, B. i.; Bergeron, J. j. Compartmentalization of SHC, GRB2 and MSOS, and Hyperphosphorylation of Raf-1 by EGF but Not Insulin in Liver Parenchyma. *The EMBO Journal* **1994**, 13 (18), 4269–4277. <https://doi.org/10.1002/j.1460-2075.1994.tb06747.x>.
- (36) Hynes, N. E.; MacDonald, G. ErbB Receptors and Signaling Pathways in Cancer. *Curr Opin Cell Biol* **2009**, 21 (2), 177–184. <https://doi.org/10.1016/j.ceb.2008.12.010>.

- (37) Lo, H.-W.; Hsu, S.-C.; Hung, M.-C. EGFR Signaling Pathway in Breast Cancers: From Traditional Signal Transduction to Direct Nuclear Translocation. *Breast Cancer Res Treat* **2006**, *95* (3), 211–218. <https://doi.org/10.1007/s10549-005-9011-0>.
- (38) Newton's Laws of Motion. *Glenn Research Center | NASA*.
- (39) Straumann, N. On Einstein's Doctoral Thesis. *arXiv:physics/0504201* **2005**.
- (40) Ronsin, C.; Muscatelli, F.; Mattei, M. G.; Breathnach, R. A Novel Putative Receptor Protein Tyrosine Kinase of the Met Family. *Oncogene* **1993**, *8* (5), 1195–1202.
- (41) Leonard, E. J.; Skeel, A. H. Isolation of Macrophage Stimulating Protein (MSP) from Human Serum. *Experimental Cell Research* **1978**, *114* (1), 117–126. [https://doi.org/10.1016/0014-4827\(78\)90043-5](https://doi.org/10.1016/0014-4827(78)90043-5).
- (42) Chao, K. L.; Tsai, I.-W.; Chen, C.; Herzberg, O. Crystal Structure of the Sema-PSI Extracellular Domain of Human RON Receptor Tyrosine Kinase. *PLoS One* **2012**, *7* (7), e41912. <https://doi.org/10.1371/journal.pone.0041912>.
- (43) Maggiora, P.; Lorenzato, A.; Fracchioli, S.; Costa, B.; Castagnaro, M.; Arisio, R.; Katsaros, D.; Massobrio, M.; Comoglio, P. M.; Flavia Di Renzo, M. The RON and MET Oncogenes Are Co-Expressed in Human Ovarian Carcinomas and Cooperate in Activating Invasiveness. *Exp Cell Res* **2003**, *288* (2), 382–389. [https://doi.org/10.1016/s0014-4827\(03\)00250-7](https://doi.org/10.1016/s0014-4827(03)00250-7).
- (44) Nitta, C. F.; Green, E. W.; Jhamba, E. D.; Keth, J. M.; Ortiz-Caraveo, I.; Grattan, R. M.; Schodt, D. J.; Gibson, A. C.; Rajput, A.; Lidke, K. A.; Steinkamp, M. P.; Wilson, B. S.; Lidke, D. S. EGFR Transactivates RON to Drive Oncogenic Crosstalk. *bioRxiv* **2020**, 2020.08.11.246785. <https://doi.org/10.1101/2020.08.11.246785>.
- (45) Yao, H.-P.; Zhou, Y.-Q.; Zhang, R.; Wang, M.-H. MSP-RON Signalling in Cancer: Pathogenesis and Therapeutic Potential. *Nat Rev Cancer* **2013**, *13* (7), 466–481. <https://doi.org/10.1038/nrc3545>.
- (46) Saxton, M. J. Single-Particle Tracking: Connecting the Dots. *Nat Methods* **2008**, *5* (8), 671–672. <https://doi.org/10.1038/nmeth0808-671>.
- (47) Ruthardt, N.; Lamb, D. C.; Bräuchle, C. Single-Particle Tracking as a Quantitative Microscopy-Based Approach to Unravel Cell Entry Mechanisms of Viruses and Pharmaceutical Nanoparticles. *Molecular Therapy* **2011**, *19* (7), 1199–1211. <https://doi.org/10.1038/mt.2011.102>.

- (48) Michalet, X.; Pinaud, F. F.; Bentolila, L. A.; Tsay, J. M.; Doose, S.; Li, J. J.; Sundaresan, G.; Wu, A. M.; Gambhir, S. S.; Weiss, S. Quantum Dots for Live Cells, in Vivo Imaging, and Diagnostics. *Science* **2005**, *307* (5709), 538–544.
<https://doi.org/10.1126/science.1104274>.
- (49) Lidke, D. S.; Lidke, K. A.; Rieger, B.; Jovin, T. M.; Arndt-Jovin, D. J. Reaching out for Signals. *J Cell Biol* **2005**, *170* (4), 619–626.
<https://doi.org/10.1083/jcb.200503140>.
- (50) Liu, D.; Liu, C.; Hu, J.; Hang, L.; Li, X.; Wei, Y.; Zhu, H.; Zhang, Q.; Wang, X. Construction and Evaluation of HA-Epitope-Tag Introduction onto the VP1 Structural Protein of a Novel HY12 Enterovirus. *Virology* **2018**, *525*, 106–116.
<https://doi.org/10.1016/j.virol.2018.09.010>.
- (51) Saxton, M. J.; Jacobson, K. Single-Particle Tracking: Applications to Membrane Dynamics. *Annu Rev Biophys Biomol Struct* **1997**, *26*, 373–399.
<https://doi.org/10.1146/annurev.biophys.26.1.373>.
- (52) A spatially restricted increase in receptor mobility is involved in directional sensing during Dictyostelium discoideum chemotaxis | Journal of Cell Science
<https://jcs.biologists.org/content/121/10/1750> (accessed 2021 -01 -18).
- (53) Rabiner, L.; Juang, B.-H. *Fundamentals of Speech Recognition*; Prentice-Hall, Inc.: USA, 1993.
- (54) Eddy, S. R. Hidden Markov Models. *Curr Opin Struct Biol* **1996**, *6* (3), 361–365.
[https://doi.org/10.1016/s0959-440x\(96\)80056-x](https://doi.org/10.1016/s0959-440x(96)80056-x).
- (55) Jurafsky, D.; Martin, J. H. *Speech and Language Processing: An Introduction to Natural Language Processing, Computational Linguistics, and Speech Recognition*, 2nd ed.; Prentice Hall series in artificial intelligence; Pearson Prentice Hall: Upper Saddle River, N.J, 2009.
- (56) Schwartz, S. L.; Cleyrat, C.; Olah, M. J.; Relich, P. K.; Phillips, G. K.; Hlavacek, W. S.; Lidke, K. A.; Wilson, B. S.; Lidke, D. S. Differential Mast Cell Outcomes Are Sensitive to FcεRI-Syk Binding Kinetics. *MBoC* **2017**, *28* (23), 3397–3414.
<https://doi.org/10.1091/mbc.e17-06-0350>.
- (57) de Keijzer, S.; Serge, A.; van Hemert, F.; Lommerse, P. H. M.; Lamers, G. E. M.; Spaik, H. P.; Schmidt, T.; Snaar-Jagalska, B. E. A Spatially Restricted Increase in

- Receptor Mobility Is Involved in Directional Sensing during Dictyostelium Discoideum Chemotaxis. *Journal of Cell Science* **2008**, *121* (10), 1750–1757. <https://doi.org/10.1242/jcs.030692>.
- (58) Bharucha-Reid, A. T. *Elements of the Theory of Markov Processes and Their Applications*; Courier Corporation, 1997.
- (59) Beausang, J. F.; Zurla, C.; Manzo, C.; Dunlap, D.; Finzi, L.; Nelson, P. C. DNA Looping Kinetics Analyzed Using Diffusive Hidden Markov Model. *Biophys J* **2007**, *92* (8), L64–66. <https://doi.org/10.1529/biophysj.107.104828>.
- (60) Coelho, J. P.; Pinho, T. M.; Boaventura-Cunha, J. *Hidden Markov Models: Theory and Implementation Using MATLAB®*; CRC Press, 2019.
- (61) Hsu, P.-Y.; Liu, H.-S.; Cheng, H.-L.; Tzai, T.-S.; Guo, H.-R.; Ho, C.-L.; Chow, N.-H. Collaboration of RON and Epidermal Growth Factor Receptor in Human Bladder Carcinogenesis. *J Urol* **2006**, *176* (5), 2262–2267. <https://doi.org/10.1016/j.juro.2006.07.048>.
- (62) LoRusso, P. M.; Gounder, M.; Jalal, S. I.; André, V.; Kambhampati, S. R. P.; Loizos, N.; Hall, J.; Holzer, T. R.; Nasir, A.; Cosaert, J.; Kauh, J.; Chiorean, E. G. Phase 1 Study of Narnatumab, an Anti-RON Receptor Monoclonal Antibody, in Patients with Advanced Solid Tumors. *Invest New Drugs* **2017**, *35* (4), 442–450. <https://doi.org/10.1007/s10637-016-0413-0>.
- (63) Harrison, P. T.; Vyse, S.; Huang, P. H. Rare Epidermal Growth Factor Receptor (EGFR) Mutations in Non-Small Cell Lung Cancer. *Seminars in Cancer Biology* **2020**, *61*, 167–179. <https://doi.org/10.1016/j.semcancer.2019.09.015>.